Supplementary Information (SI) for Journal of Materials Chemistry A.

Supporting information

Facile synthesis of biomass-based sustainable covalent organic network (CON) anode for high-performance LIBs

Changyu Weng[1], Hongmei Yuan[1], Yuxin Ji[1], Weidong Liu[1], Longlong Ma[1,2], Jianguo Liu[1*]

[1] Key Laboratory of Energy Thermal Conversion and Control of Ministry of Education, School of Energy and Environment, Southeast University, Nanjing 210096, PR China.

[2] Department of Thermal Science and Energy Engineering, University of Science and Technology of China, Hefei 230026, P.R. China.

* Corresponding authors' e-mail: liujg@seu.edu.cn

Contents

1. Experimental Section

Materials

All reagents were obtained from commercial supplies and used as received. Ethyl alcohol (99.9%), 1,2-dichlorobenzene (AR), *n*-butanol (AR), *N*,*N*-dimethylacetamide (AR), propan-2-ol (AR), diformylfuran (DFF, 97%+), benzene-1,3,5-triamine trihydrochloride (TAB, 98.0%), acetic acid (HOAc, ⩾99.5%), *N*-methyl-2-pyrrolidinone (NMP, 99.5%), tetrahydrofuran (THF, 99.5%), and methanol (99.9%), carbon nanotubes (CNT, purity:>95 wt%, OD:<2nm, length:1-3 μm) were purchased from Tansoole. The acetone (99.0%) was purchased from Sinopharm Chemical Reagent Limited Corporation. Acetylene black and polyvinylidene fluoride (PVDF) were purchased from Canrd.

Material Characterization

The synthesis of the samples was verified using Fourier transform infrared spectroscopy (FT-IR, Nicolet IS50, Thermo Fisher Scientific). The crystalline structure of the samples was studied using X-ray diffractometry (XRD, Smartlab (3), Rigaku). The microstructure was investigated using a scanning electron microscope (SEM, Nova Nano SEM450, FEI) and transmission electron microscope (TEM, Talos F200X, Thermo Fisher Scientific). The system of Thermo Scientific K-Alpha was employed to obtain X-ray photoelectron spectroscopy (XPS) spectra. The values of binding energy were calibrated by using C 1s peak at 284.8 eV. The initial electrodes used for the XPS measurement were tested after being immersed in the electrolyte for 48 hours. This step was taken to eliminate the interference of the electrolyte on the electrodes under different charge-discharge conditions. By doing so, we aimed to ensure that the XPS results accurately reflected the characteristics of the electrodes themselves rather than being affected by the electrolyte's impact during the measurement process. Nitrogen adsorption and desorption isotherms were measured at 77 K using a Micromeritics 3Flex. The samples were degassed at 120 °C for 10 h before the measurements. Surface areas were calculated from the adsorption data using Brunauer-Emmett-Teller (BET). Thermogravimetric analysis (TGA) was carried out on TG209 F3 by heating samples from 30 to 900 °C in a dynamic nitrogen atmosphere with a heating rate of 10 $°C \cdot min^{-1}$. The ^{13}C cross-polarization solid-state nuclear magnetic resonance (^{13}C CP/MS NMR) spectrum was performed by Bruker-500. The elemental analysis was studied using a Vairo EL cube.

Density functional theory (DFT) calculation

The theoretical calculations were based on the DFT using the CASTEP, Dmol3 and Reflex tools modules of Materials Studio (MS) software. The function of CASTEP was chosen as Perdew-BurkeErnzerh (PBE) in generalized gradient approximation (GGA).

The weight ratio of CON and CNT in CON@CNT

The weight ratio of CON and CNT in the CON@CNT was investigated based on the N and C contents in the pristine CON, the CNT, and the CON@CNT, as shown in Table S2. The two equations can be described as follows:

$$P_{\mathrm{CON}} \times N_{\mathrm{CON}} + P_{\mathrm{CNT}} \times N_{\mathrm{CNT}} = N_{\mathrm{CON@CNT}}$$

$$P_{\mathrm{CON}} \times C_{\mathrm{CON}} + P_{\mathrm{CNT}} \times C_{\mathrm{CNT}} = C_{\mathrm{CON@CNT}}$$

Where N_{CON} and C_{CON}, N_{CNT} and C_{CNT}, $N_{\mathrm{CON@CNT,}}$ and $C_{\mathrm{CON@CNT}}$ correspond to the weight percentages of N and C in pristine CON, pristine CNT, and the CON@CNT composite, respectively, P_{CON} and P_{CNT} correspond to the mass percentages of CON and CNT in the CON@CNT composite.

Capacity contribution of CON in CON@CNT calculation

The composite capacity of CON@CNT can be regarded as the contribution of two components, as described by the following equation:

$$C_{\mathrm{CON@CNT}} = C_{\mathrm{CON}} \times P_{\mathrm{CON}} + C_{\mathrm{CNT}} \times P_{\mathrm{CNT}}$$

where $C_{\mathrm{CON@CNT}}$, C_{CON}, and C_{CNT} represent the capacities of CON@CNT, CON, and CNT, respectively. P_{CON} and P_{CNT} correspond to the mass percent of CON and CNT in the CON@CNT composite.

The theoretical capacity of the CONs

The theoretical capacity of the material can be compartmentalized based on the number of lithium interacting with the specific binding sites present within the CON framework. For establishing the different lithium binding sites present within the CON, we had analyzed the MESP of CON framework via DFT. Typical theoretical capacity (C_t) of a material is given by the equation:

$$C_t = n \times F/(3600 \times M_w/1000) \approx n \times 26800/M_w$$

where n is the number of Li-ions per monomer, F and M_w are Faraday constant and molecular weight per active species, respectively. The M_w of the BIO was 510 g/mol. Consequently, when n=11, the C_t was calculated to be 578 mAh g^{-1}. Conversely, when n=10, the C_t was found to be 525 mAh g^{-1}.

2. Procedures for CON materials Synthesis

Synthesis of BIO under the optimal condition

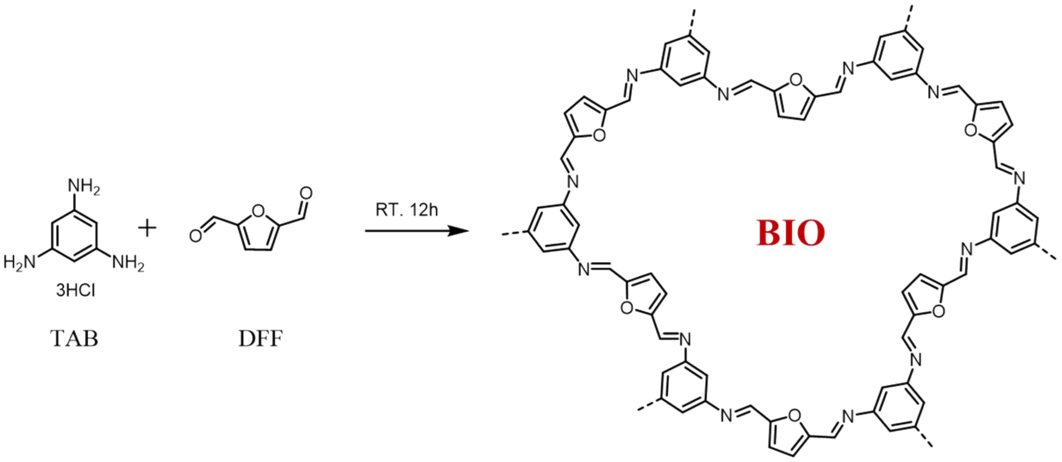

Benzene-1,3,5-triamine trihydrochloride (TAB (46.5 mg, 0.2 mmol)) and diformylfuran (DFF (37.2 mg, 0.3 mmol)) were suspended in a mixture of *N*,*N*-dimethylacetamide/propan-2-ol (1:1 V: V, 3 mL). After the mixture was sonicated for 20 min, the reaction tube was sealed and kept at room temperature for 12h. The resulting BIO precipitate was isolated by vacuum filtration, washed with THF, methanol, and acetone, and dried at 60 °C under vacuum for 12 hours to give the desired BIO.

Synthesis of BIO under the other condition

The detailed synthesis of the materials under the conventional condition of solvothermal synthesis (entry a-f) are as follows: TAB (46.5 mg, 0.2 mmol) and DFF (37.2 mg, 0.3 mmol) were suspended in a mixture of solvents (Table S1). After the mixture was sonicated for 20 minutes, acetic acid (6 M, 0.2 ml) was added. Subsequently, the Pyrex tube was frozen at 77 K using a liquid N_2 bath and degassed by three freeze-pump-thaw cycles, then sealed under vacuum and heated at 120 °C for 72 hours. The precipitate of the resulting materials was isolated by vacuum filtration and washed with THF, methanol, and acetone, then dried at 100 °C under vacuum for 24 hours to give the products.

The detailed synthesis of the materials under the mild conditions (entry g-i) are as follows: TAB (46.5 mg, 0.2 mmol) and DFF (37.2 mg, 0.3 mmol) were suspended in a mixture of solvents. After the mixture was sonicated for 20 min, the reaction tube was sealed and kept at room temperature for 12h. The resulting materials precipitate was isolated by vacuum filtration and washed with THF, methanol and acetone, then dried at 60 °C under vacuum for 12 hours to give the products.

Table S1 The detailed synthesis of the materials under different conditions.

Entry	Solvent	Catalyst	Temperature	Time	Yield	Crystallinity
a	*n*-Butanol/1,2-dichlorobenzene=1.5ml/1.5ml	0.2 ml 6M HOAc	120℃	72h	low	low
b	ethyl alcohol/1,2-dichlorobenzene=1.5ml/1.5ml	0.2 ml 6M HOAc	120℃	72h	low	high
c	ethyl alcohol=2ml	0.2 ml 6M HOAc	120℃	72h	high	low
d	N,N-dimethylacetamide/propan-2-ol=1.5ml/1.5ml	0.2 ml 6M HOAc	120℃	72h	high	low
e	propan-2-ol=2ml	0.2 ml 6M HOAc	120℃	72h	low	high
f	N,N-dimethylacetamide=2ml	0.2 ml 6M HOAc	120℃	72h	low	low
g	ethyl alcohol/1,2-dichlorobenzene=1.5ml/1.5ml	/	25℃	12h	low	high
h	ethyl alcohol=2ml	/	25℃	12h	low	high
i	N,N-dimethylacetamide/propan-2-ol=1.5ml/1.5ml	/	25℃	12h	**high**	**high**

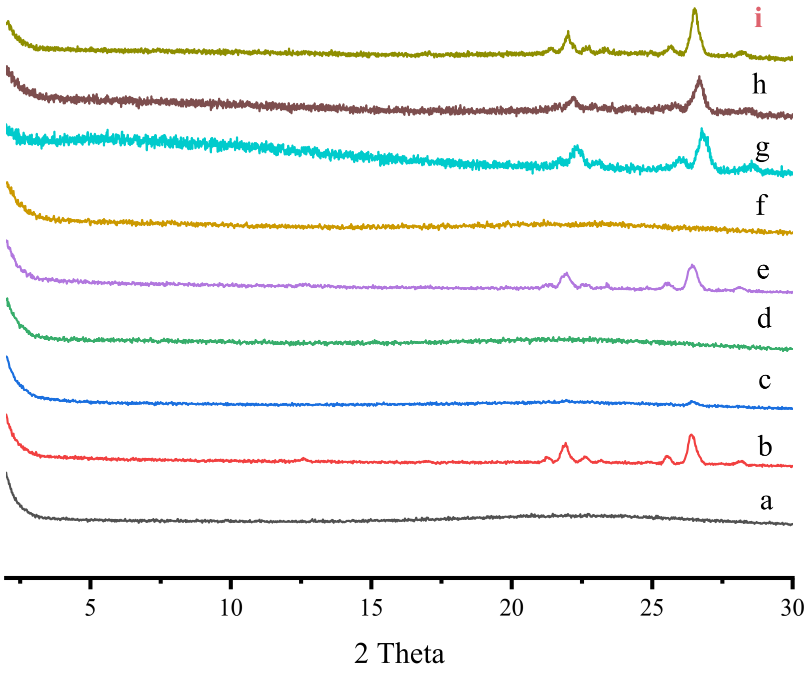

Fig. S1 XRD patterns of materials under different conditions.

Synthesis of BIO-X (X=2C, 4C)

The BIO-X was prepared using a similar synthesis method with BIO under the optimal condition. The only difference was that the CNT (BIO-2C: 16.7 mg; BIO-4C: 33.5 mg) was added at the same time as TAB (46.5 mg, 0.2 mmol) and DFF (37.2 mg, 0.3 mmol). The other processes were consistent with those used to prepare BIO.

Synthesis of BIO/4C

BIO/40 was synthesized through a simple physical mixing technique. The BIO with 42.7 mg and CNT with 57.3 mg were transferred to a mortar and ground for a 30-minute grind to obtain homogeneous composites.

3. Electrochemical Measurements

Coin-type (CR2032) cells were assembled in an Ar-filled glove box ($H_2O < 0.1$ ppm, $O_2 < 0.1$ ppm) with lithium metal foil as the anode and Celgard 2325 as the separator. The electrolyte was 1.0 M $LiPF_6$ in a mixture of dimethyl carbonate (DMC) and ethylene carbonate (EC) (1:1 v/v). The active materials (BIO and BIO-X) were mixed with acetylene black and polyvinylidene fluoride binder (PVDF) solution in a weight ratio of 6:3:1 in *N*-methyl-2-pyrrolidinone (NMP), respectively. The slurry was cast on the Cu foil and dried for 10 h at 100 °C under a vacuum to remove NMP. The discharge and charge measurements were carried out on a Land instruments CT3001A testing system at various current densities of 100-2,000 mA g^{-1} with a cut-off voltage of 0.005-3.0 V vs Li^+/Li. Cyclic voltammetry (CV) and electrochemical impedance spectroscopy (EIS) measurements were conducted using the coin cells on a CHI 760E electrochemical workstation.

4. Elemental Analysis

Table S2 Elemental analysis results of pristine CON, CNT, and CON@CNT

Samples	C (%)	N (%)	H (%)
BIO	43.635	16.342	4.568
BIO-4C	65.821	7.326	2.482
CNT	82.282	0.647	0.702

5. X-ray Diffraction (XRD)

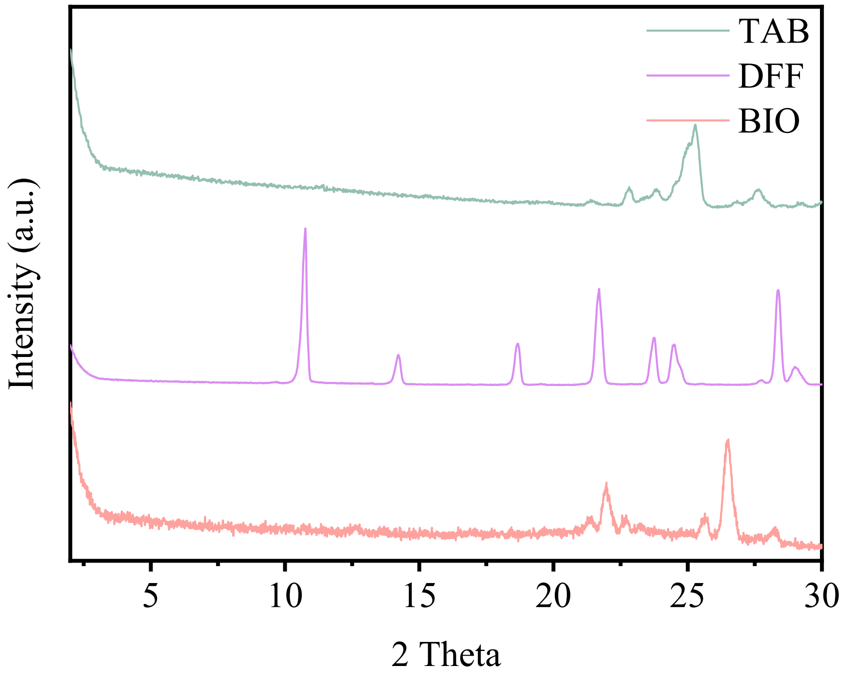

Fig.S2 Experimental XRD patterns of the BIO, TAB, and DFF.

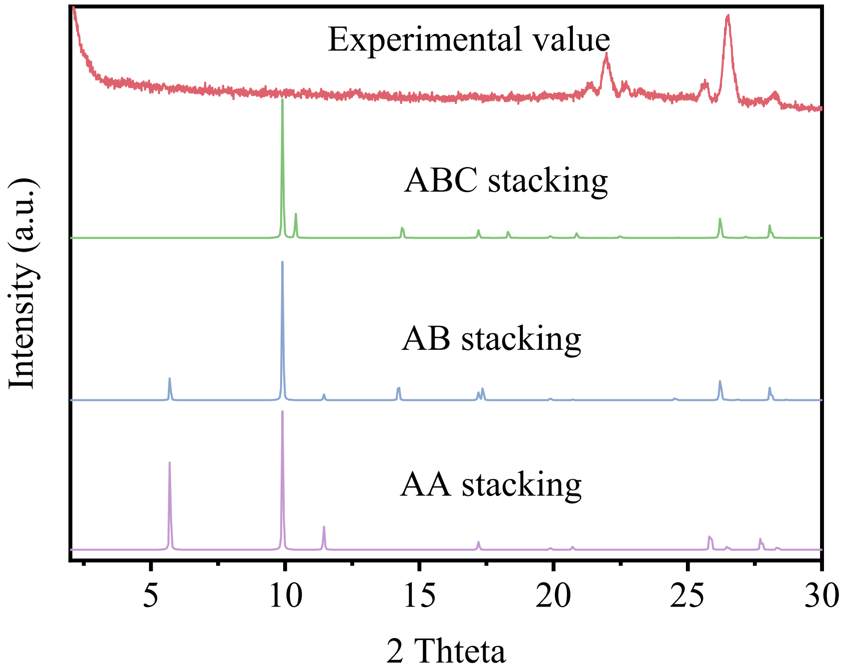

Fig.S3 Experimental and simulated XRD patterns of the BIO

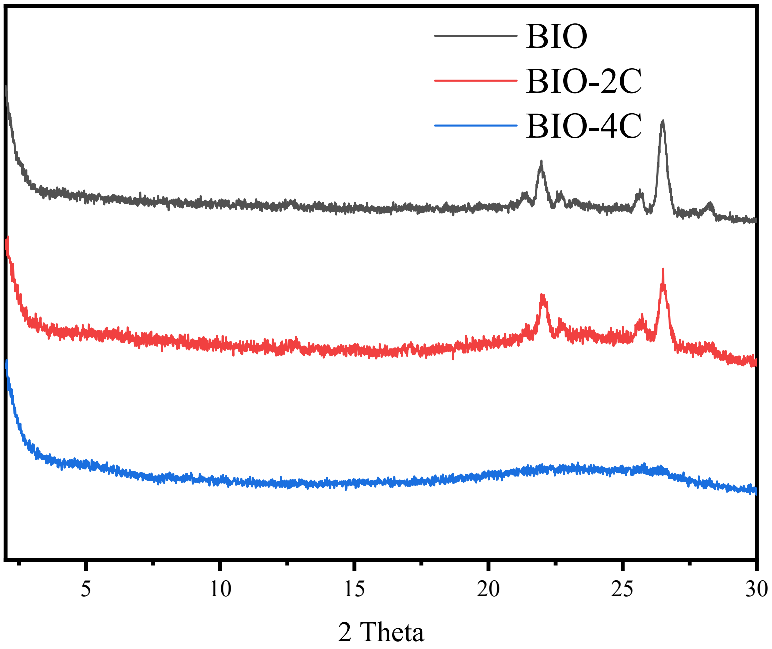

Fig. S4 XRD patterns of BIO, BIO-2C, and BIO-4C

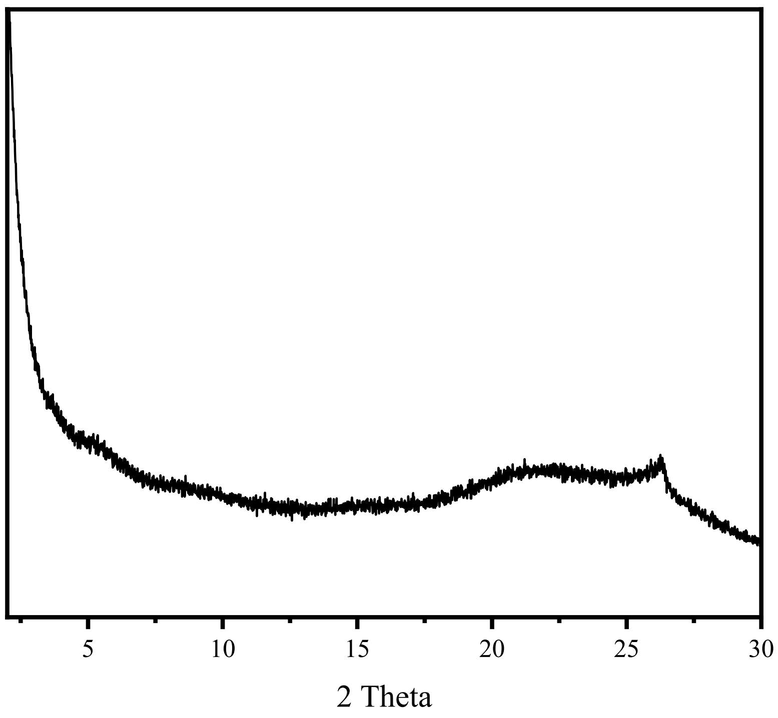

Fig. S5 XRD patterns of pure CNT.

6. Nitrogen Adsorption-Desorption Isotherms

Table S3. Structural properties of CON, CON@CNT composite, and CNT calculated based on nitrogen adsorption analysis.

Sample name	BET (m^2/g)
BIO	19
BIO-2C	13
BIO-4C	17
CNT	294

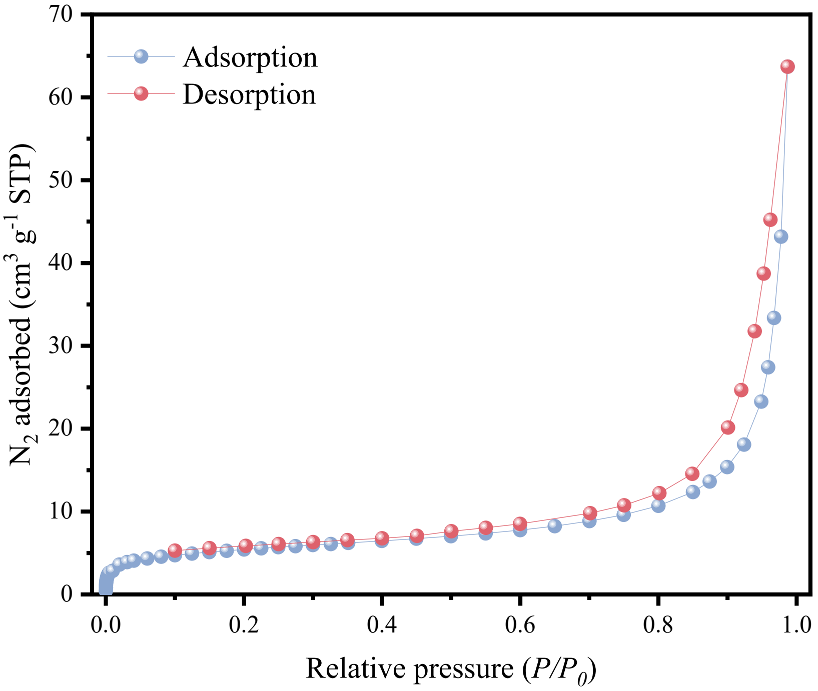

Fig. S6 Nitrogen adsorption-desorption isotherms of BIO.

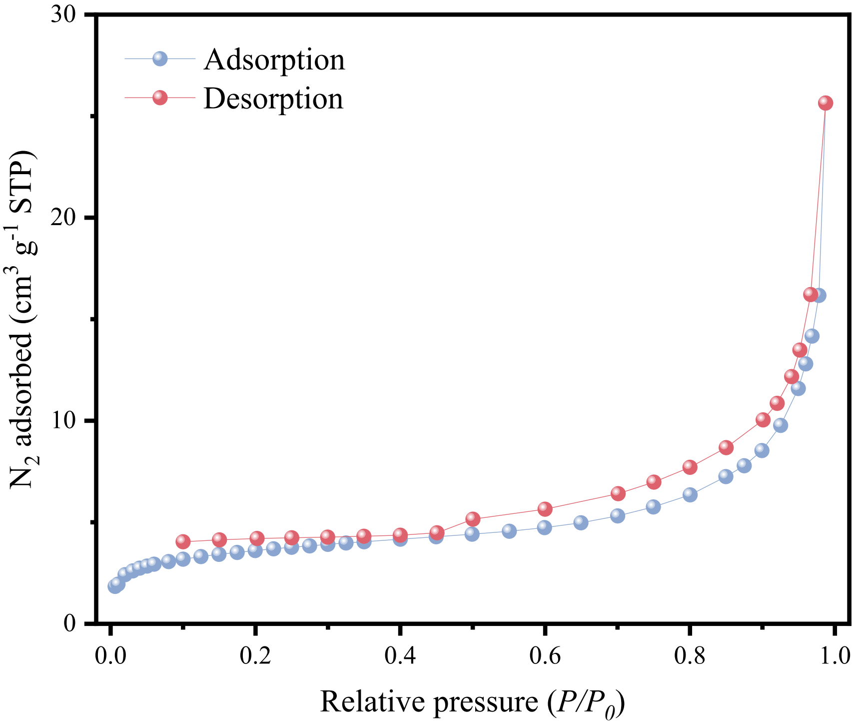

Fig. S7 Nitrogen adsorption-desorption isotherms of BIO-2C.

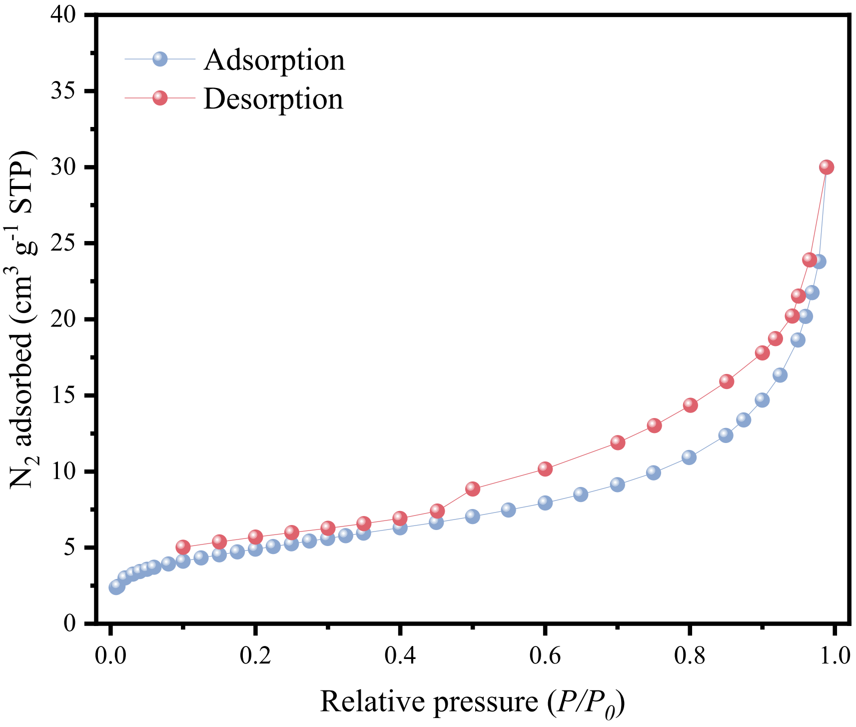

Fig. S8 Nitrogen adsorption-desorption isotherms of BIO-4C.

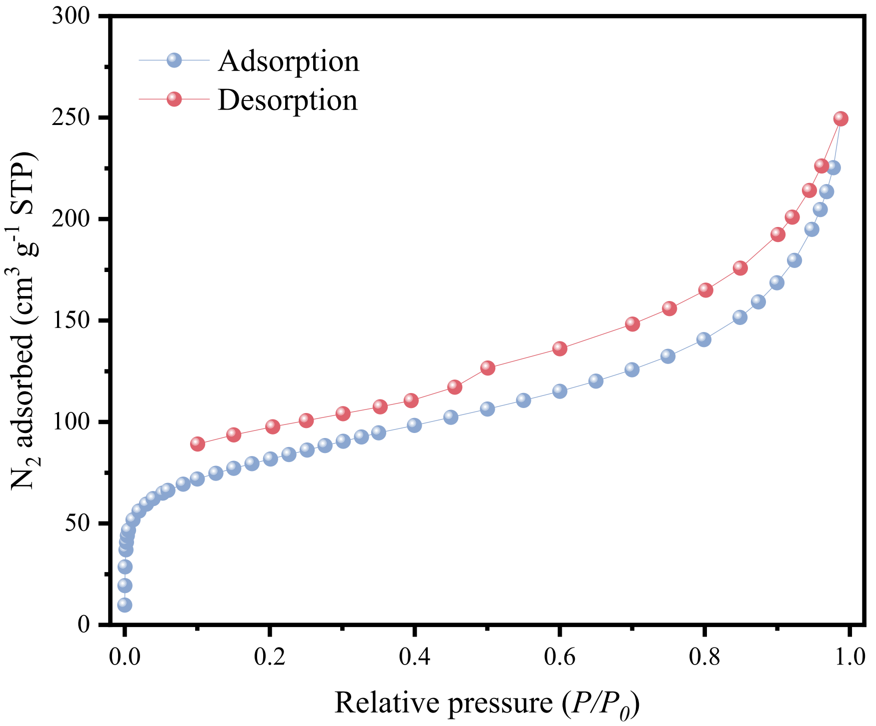

Fig. S9 Nitrogen adsorption-desorption isotherms of CNT.

7. Scanning Electron Microscope

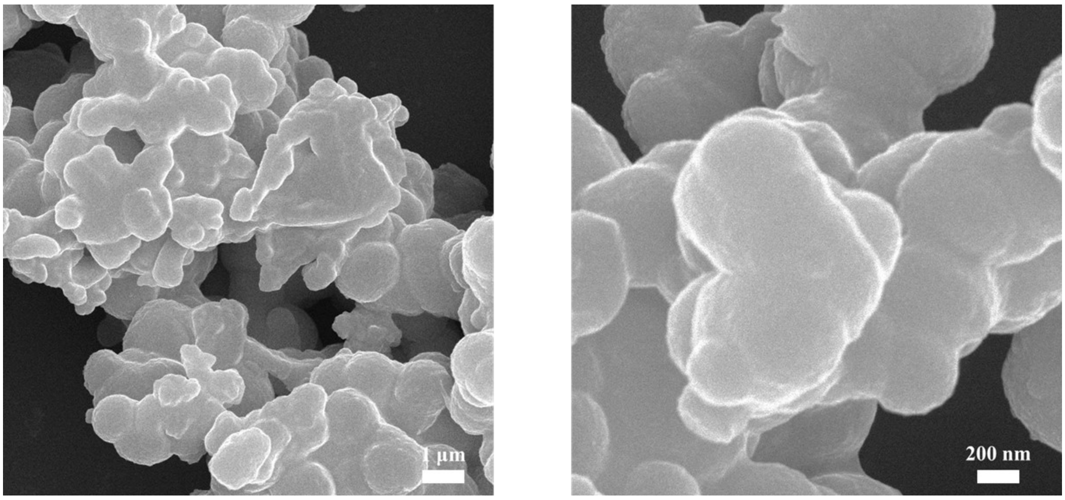

Fig. S10 SEM images of BIO

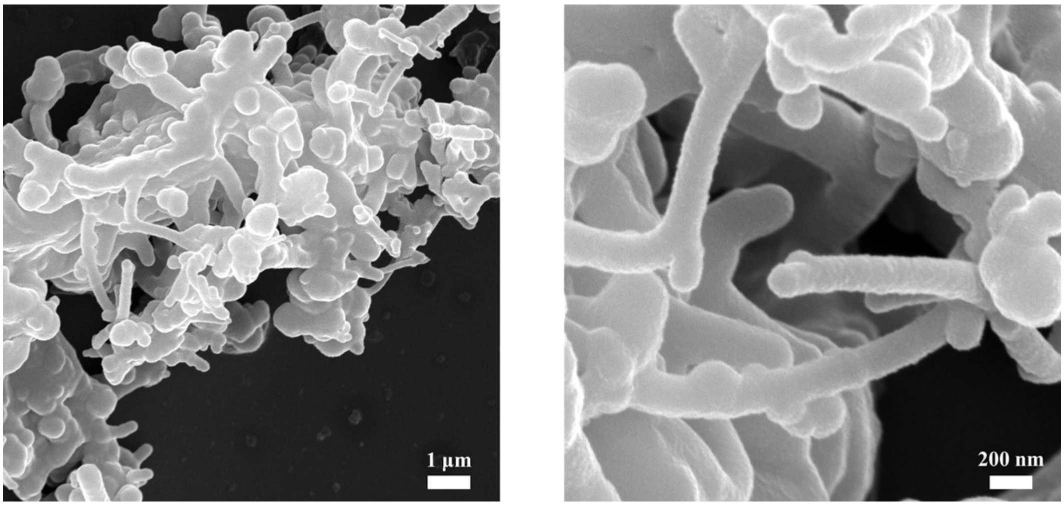

Fig. S11 SEM images of BIO-2C

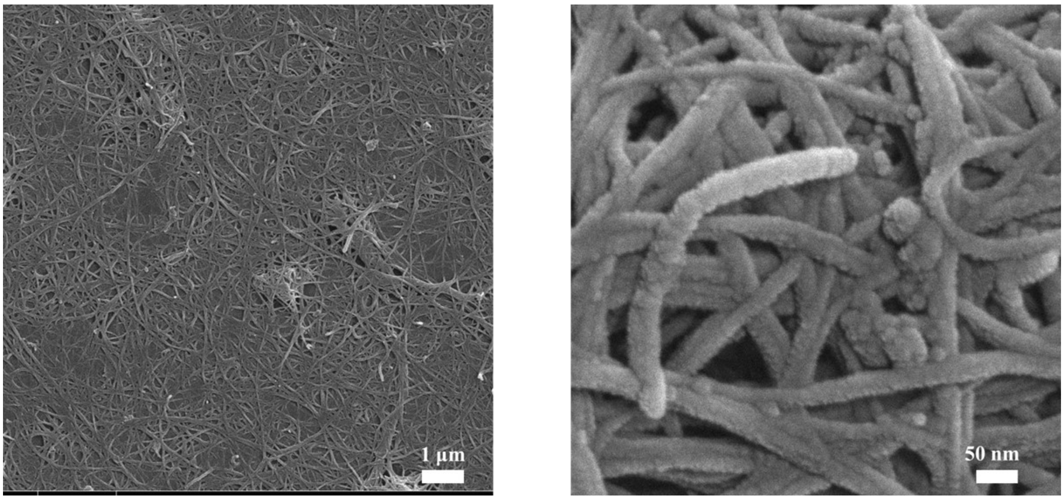

Fig. S12 SEM images of CNT

8. High-Resolution Transmission Electron Micrographs

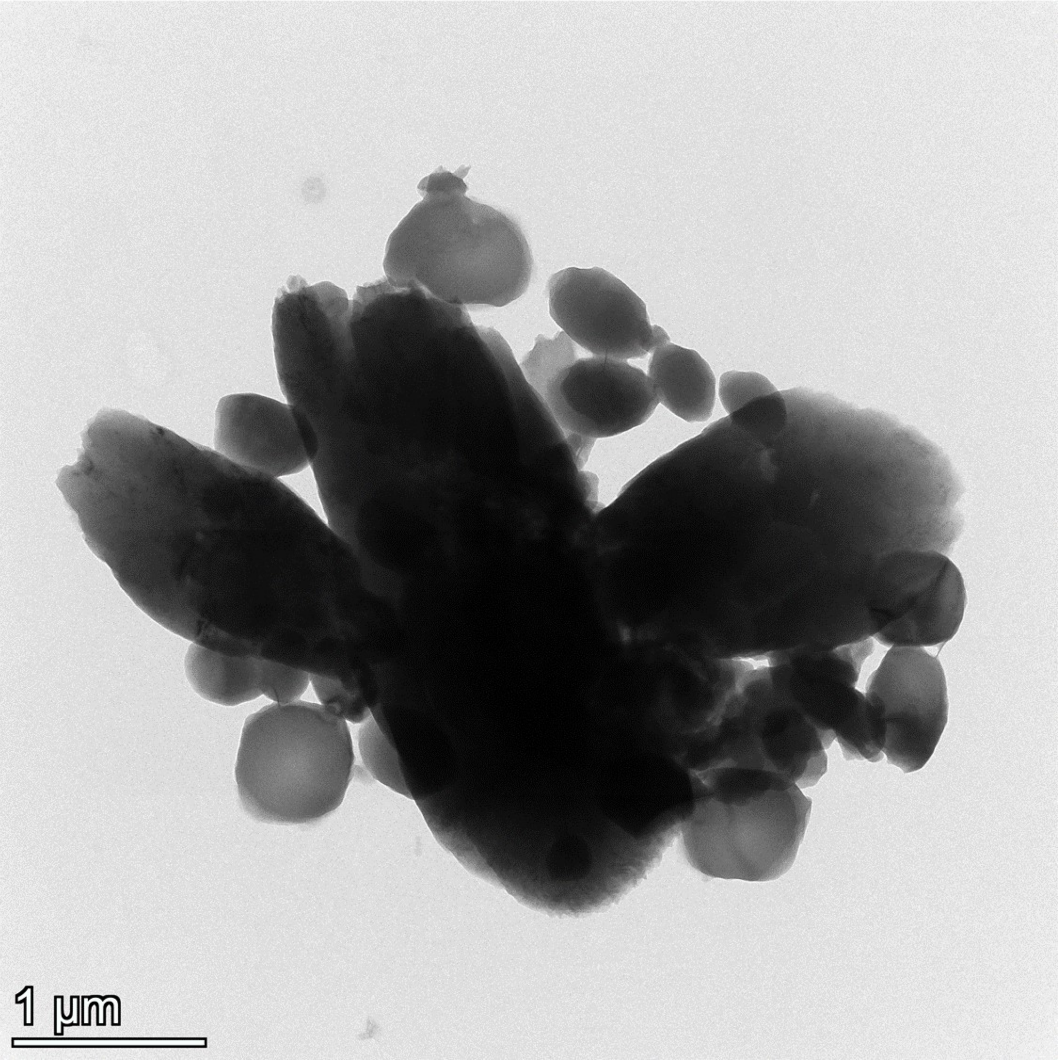

Fig. S13 HRTEM images of BIO

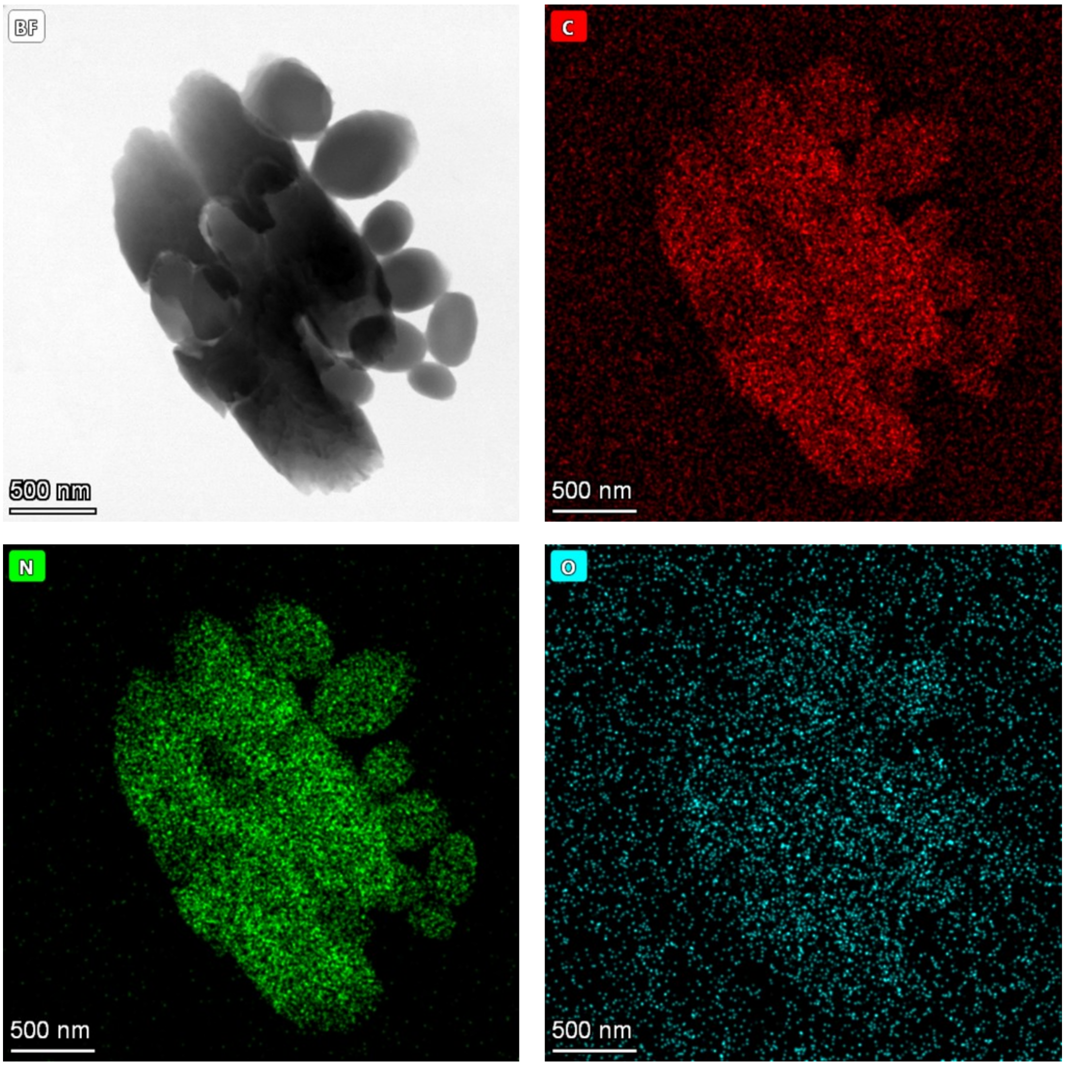

Fig. S14 EDS elemental mappings of BIO

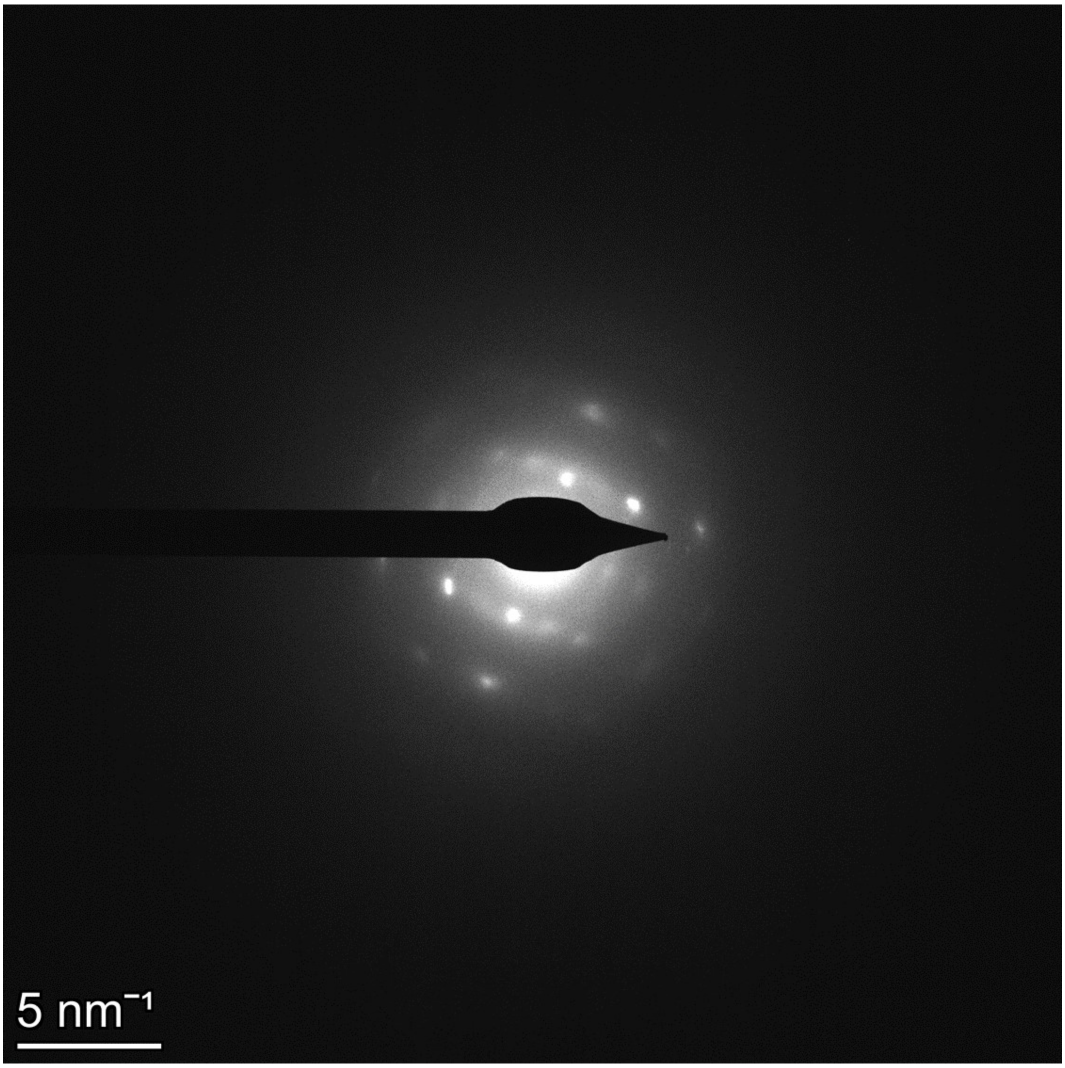

Fig. S15 HRTEM images of BIO with SAED pattern

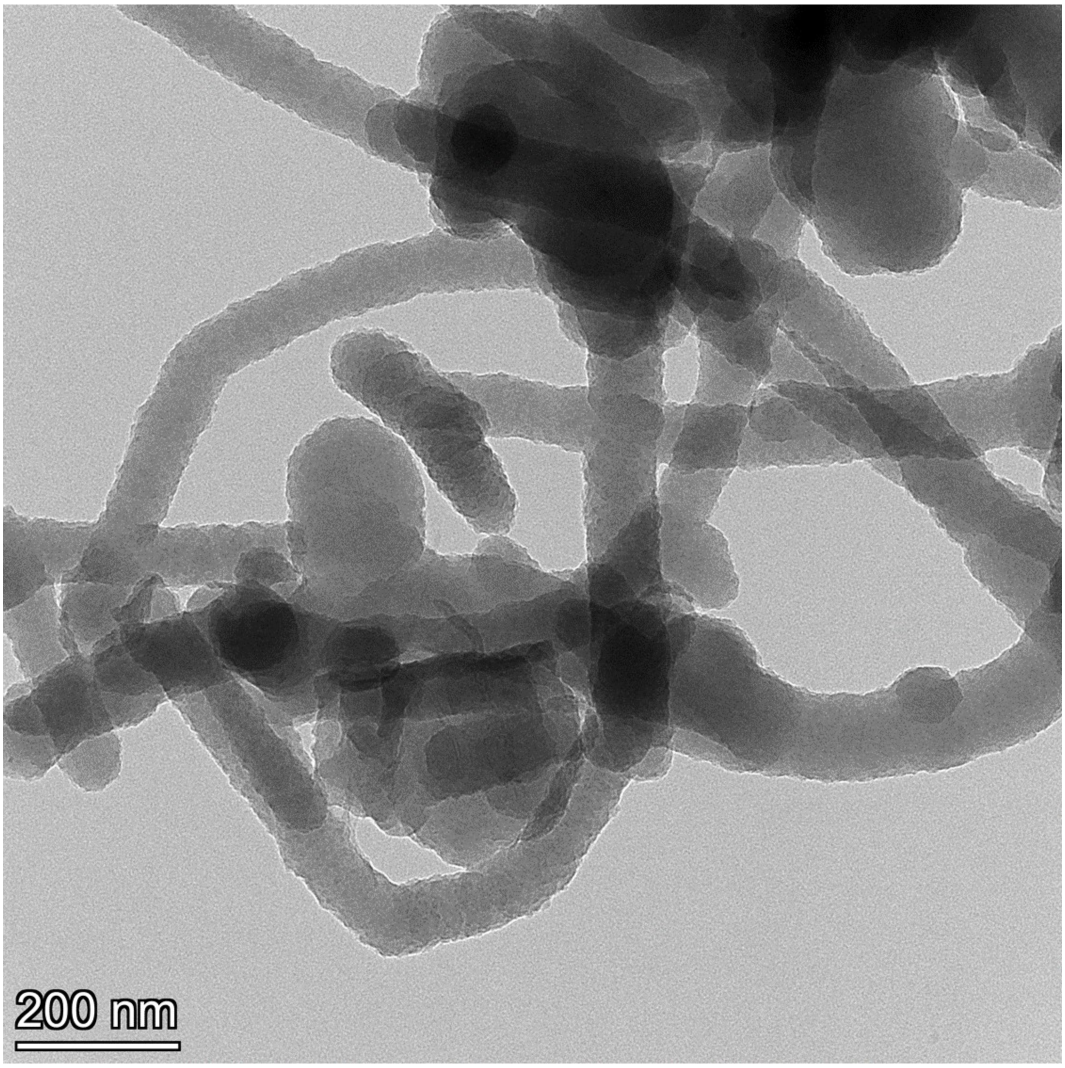

Fig. S16 HRTEM images of BIO-2C

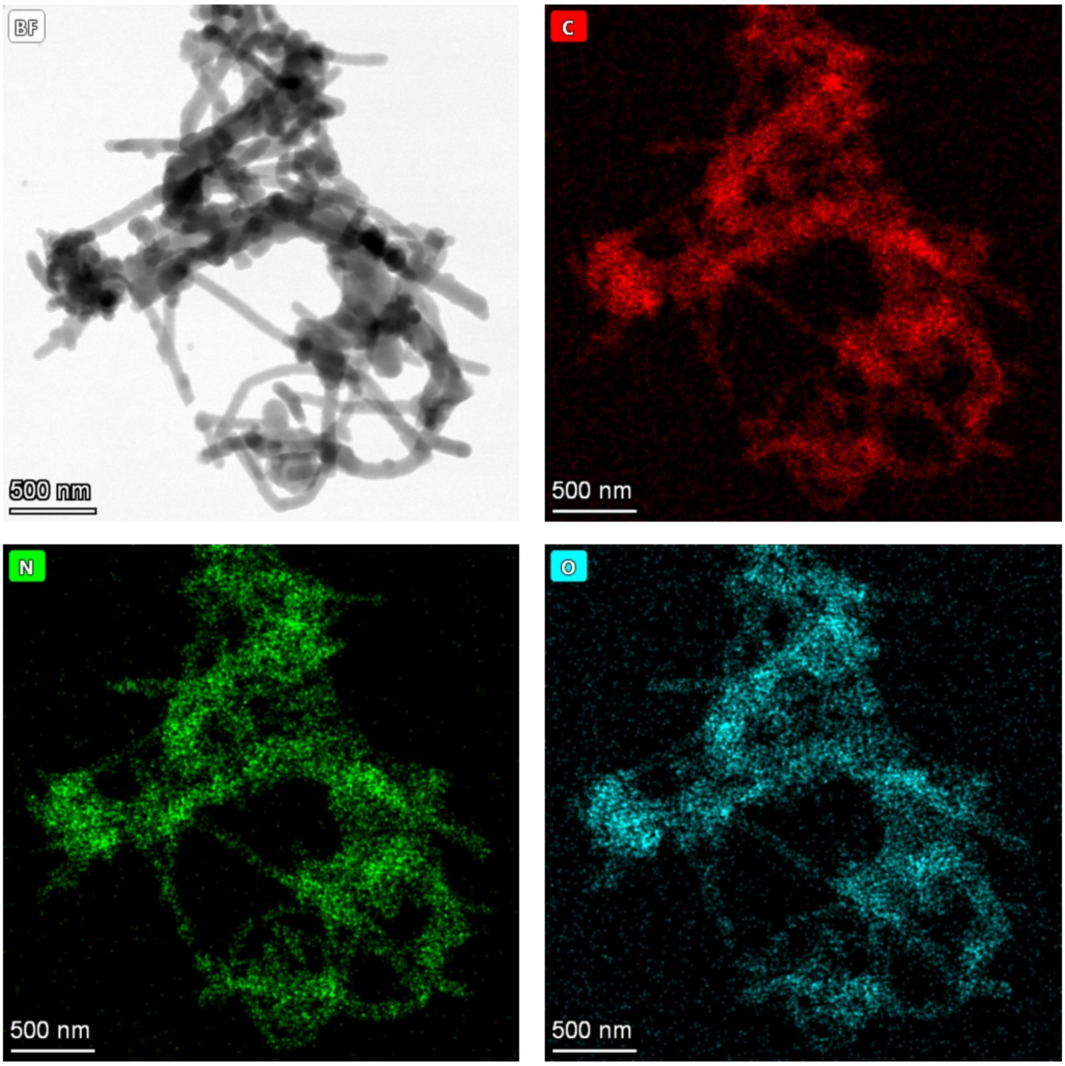

Fig. S17 EDS elemental mappings of BIO-2C

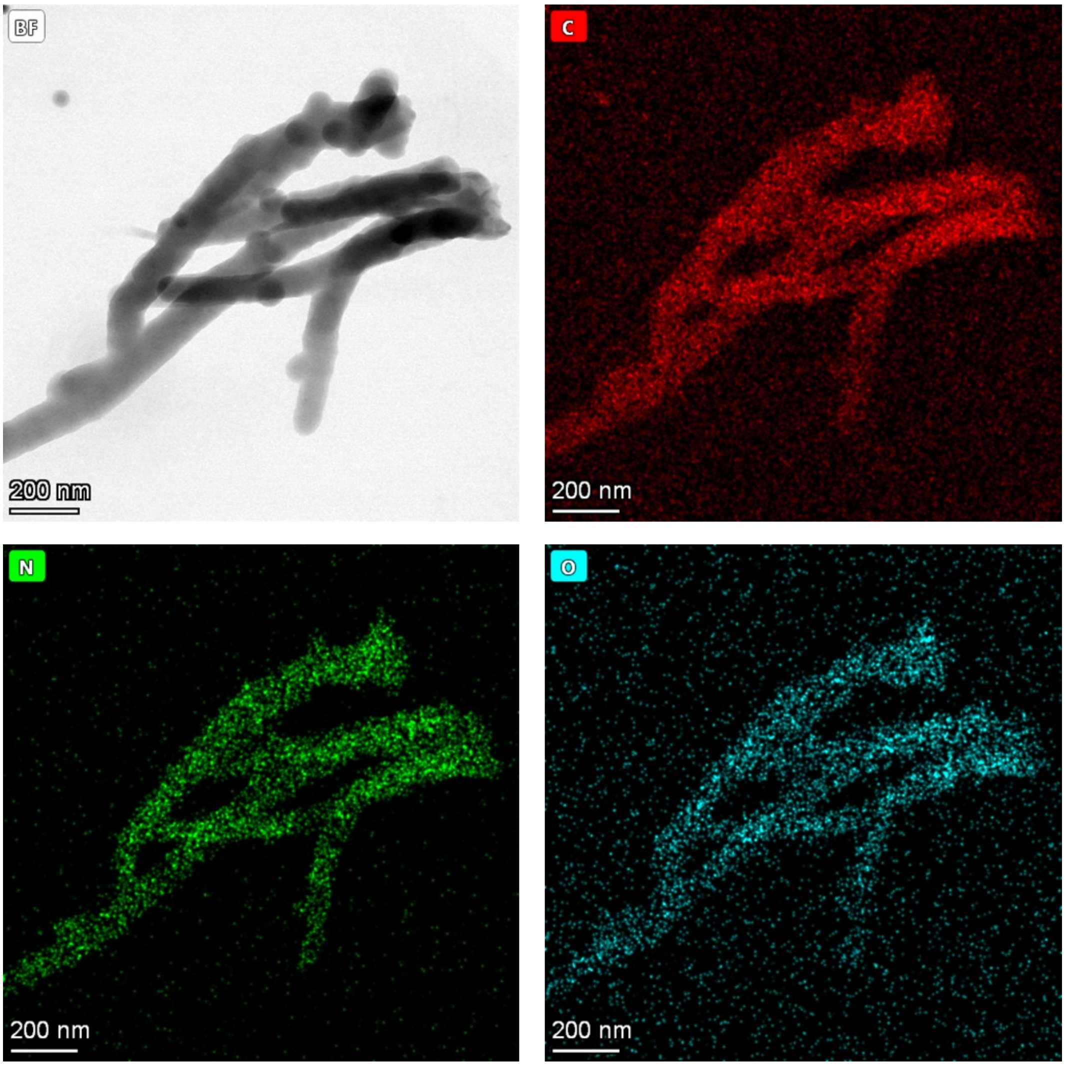

Fig. S18 EDS elemental mappings of BIO-4C

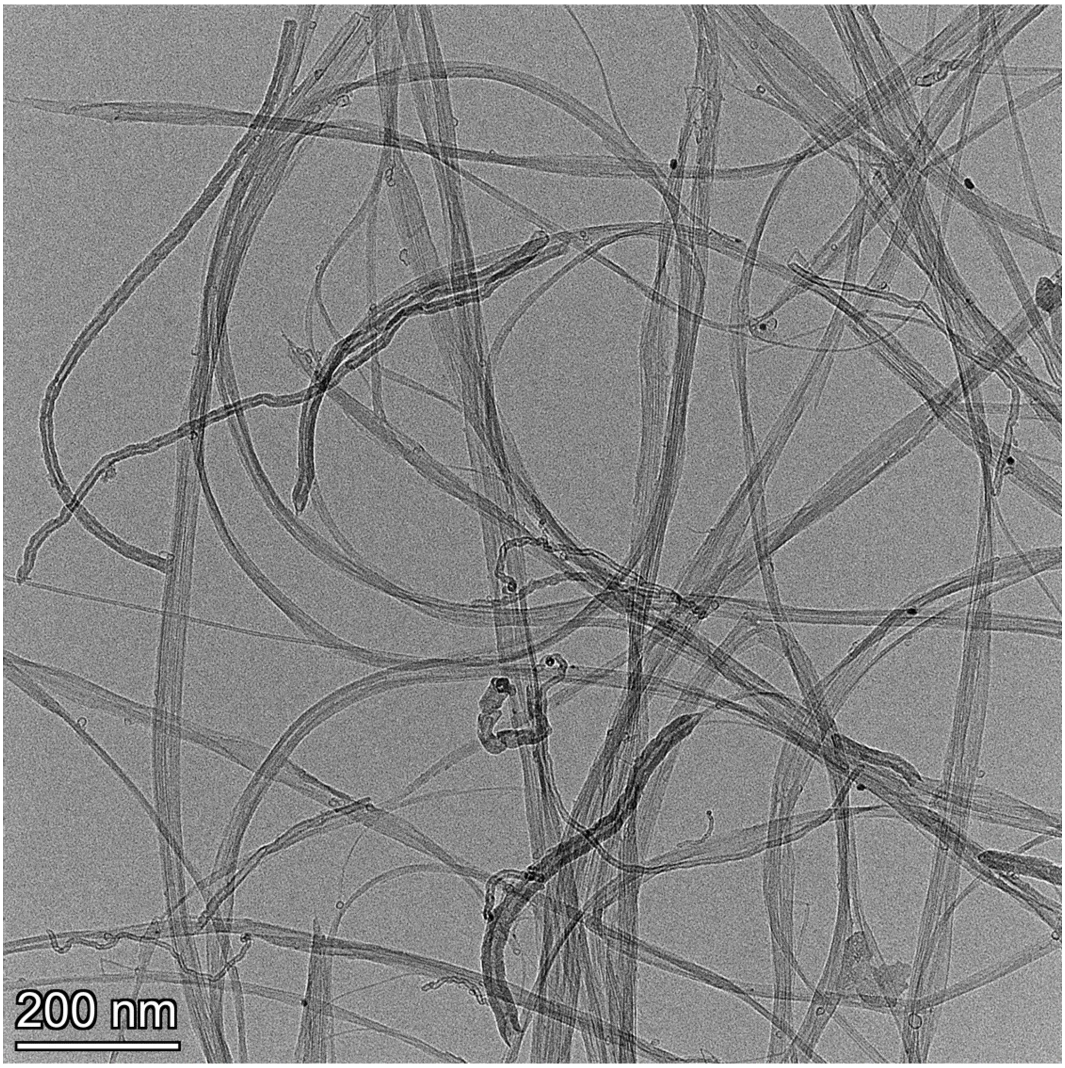

Fig. S19 HRTEM images of CNT

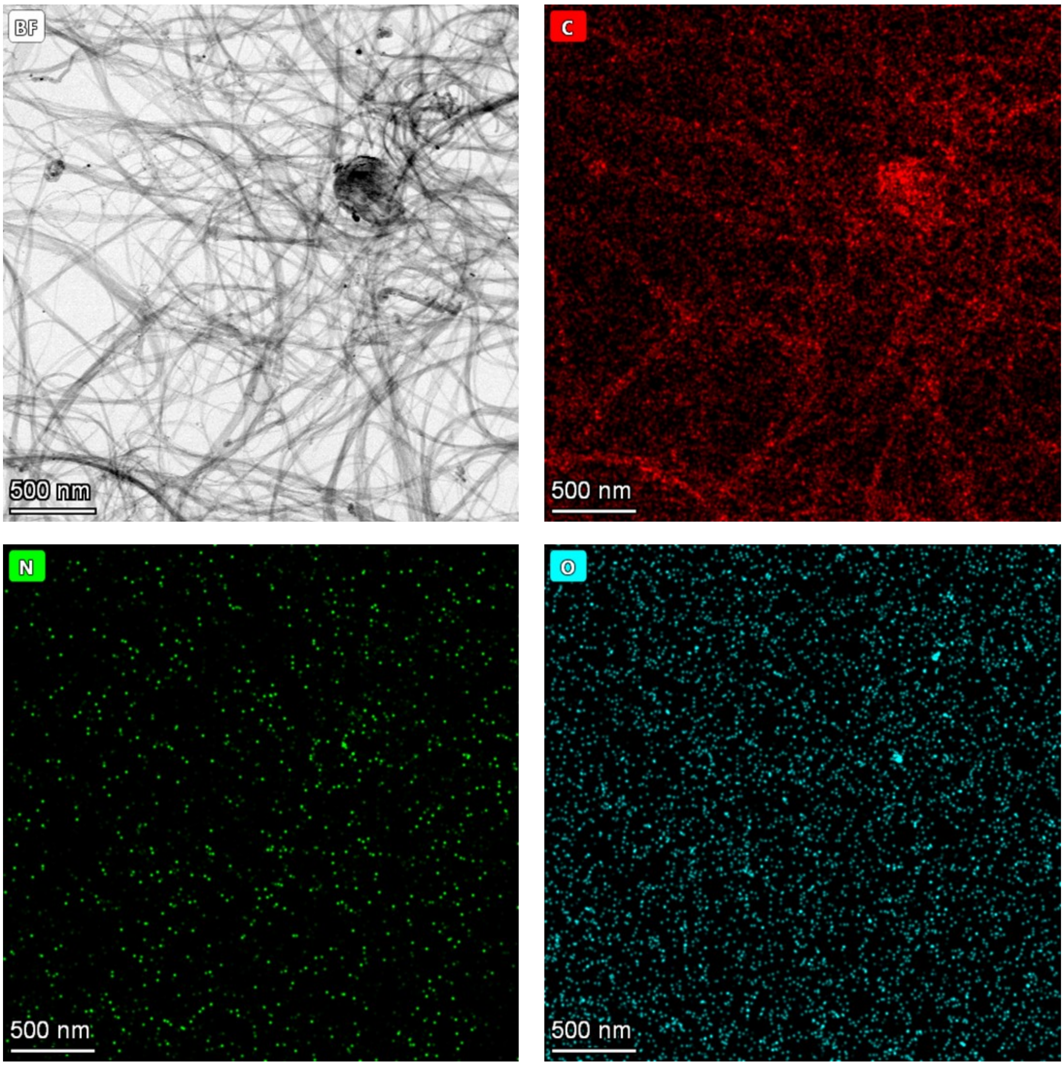

Fig. S20 EDS elemental mappings of CNT

9. Electrochemical Performance

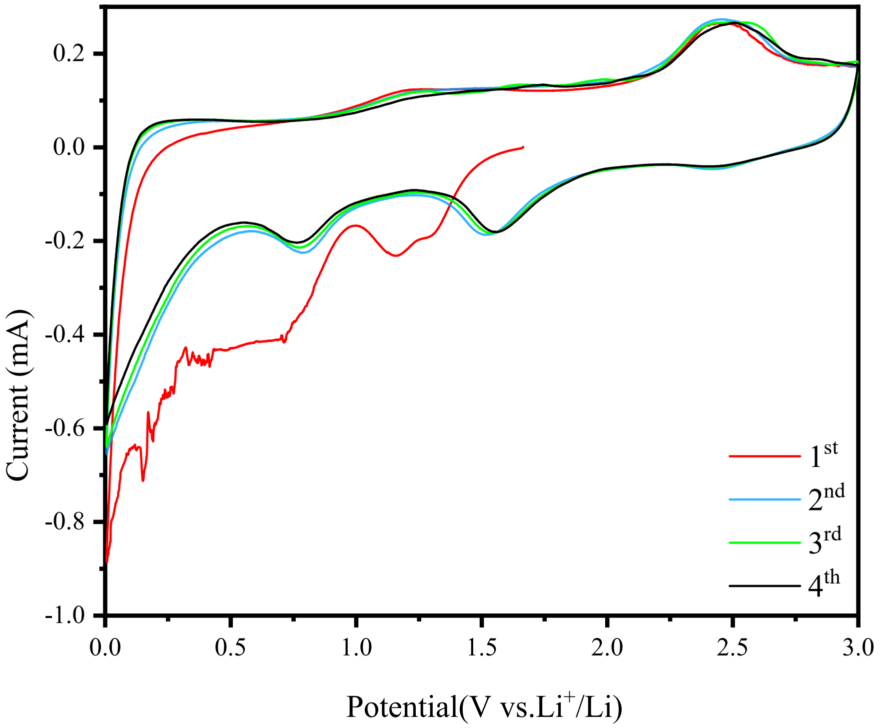

Fig. S21 The first four cycles of cyclic voltammograms of the BIO-4C-based electrode

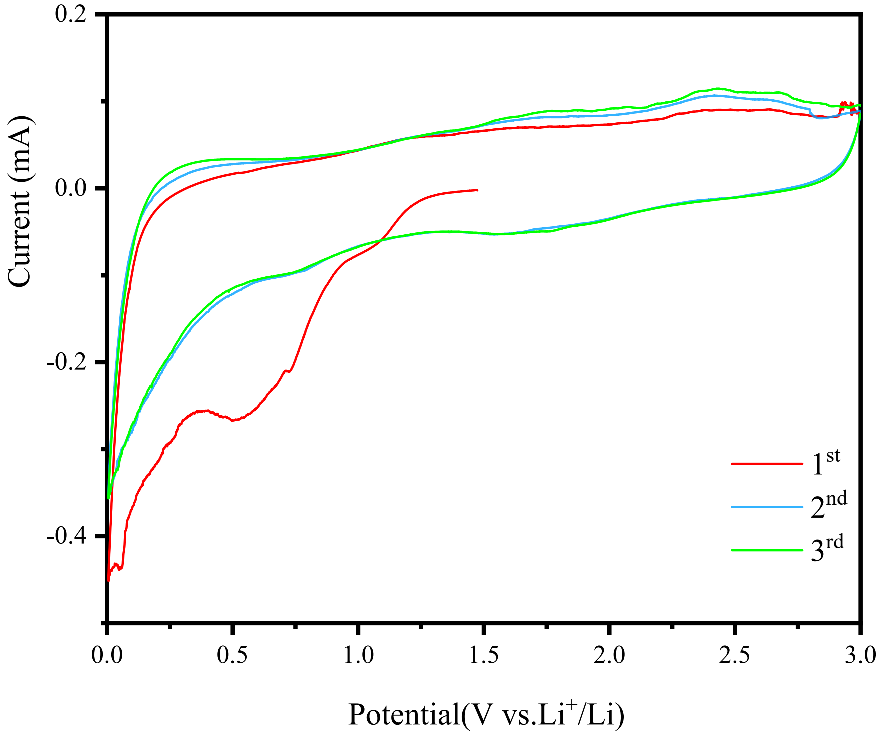

Fig. S22 The first three cycles of cyclic voltammograms of the BIO-2C-based electrode

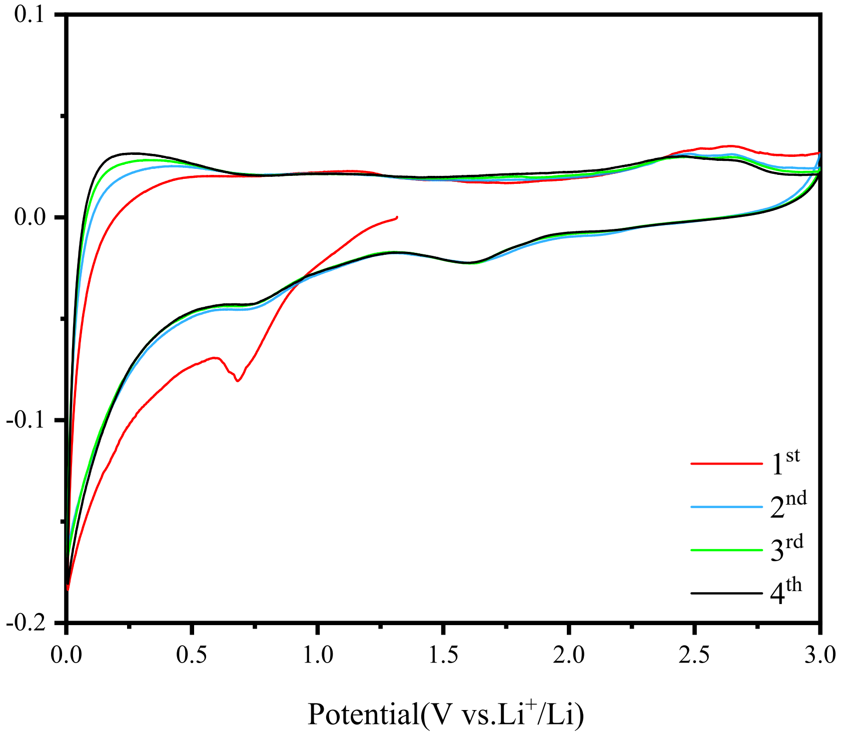

Fig. S23 The first four cycles of cyclic voltammograms of the pure BIO-based electrode

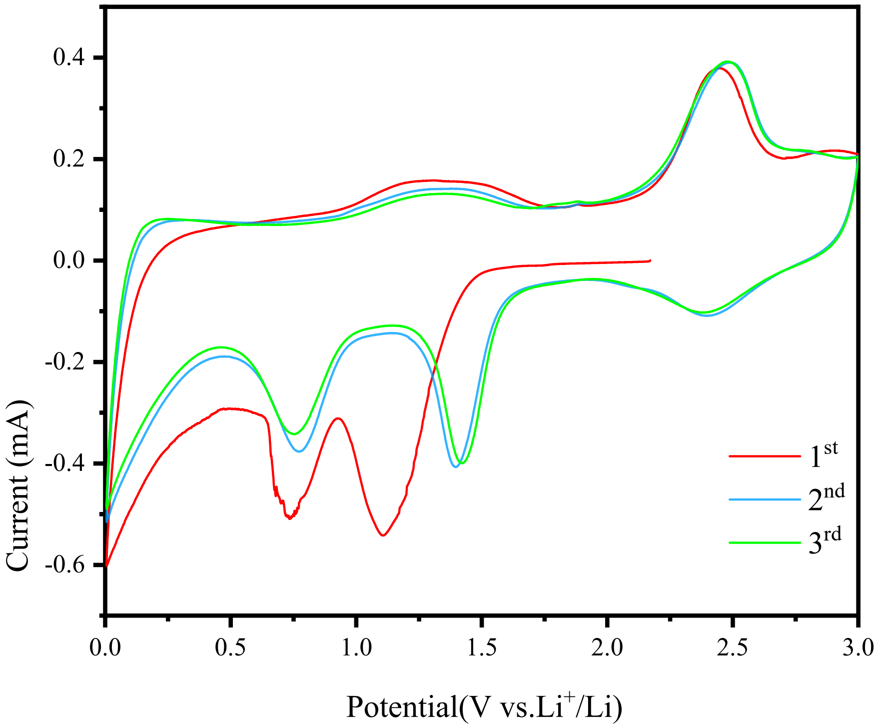

Fig. S24 Voltage-capacity curves of the first three cycles of cyclic voltammograms of the BIO/4C-based electrode

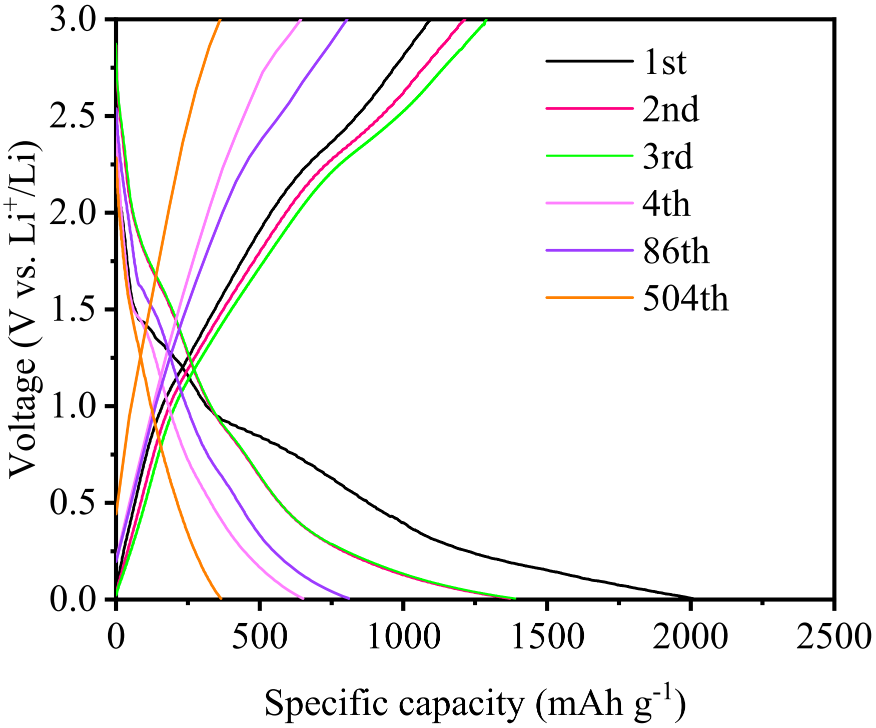

Fig. S25 BIO-4C at 100 mA g^{-1} for the first three cycles and the 4th, 86th, and 504th under the 2000 mA g^{-1}

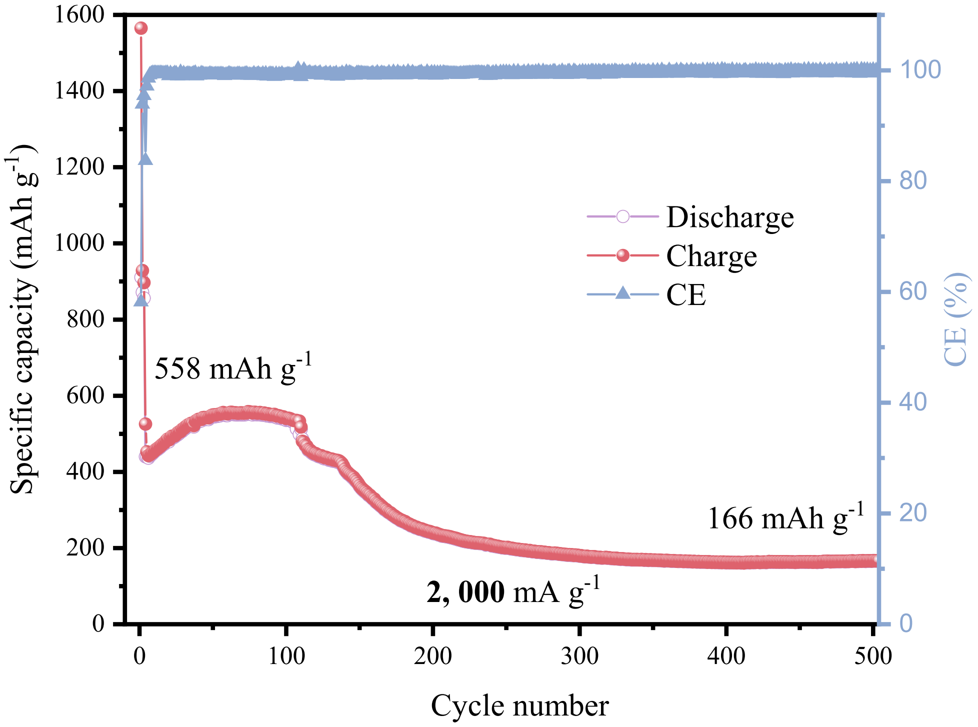

Fig. S26 Long-term cycle performances of the BIO-2C anode at 2,000 mA g-1 after three-cycle activation.

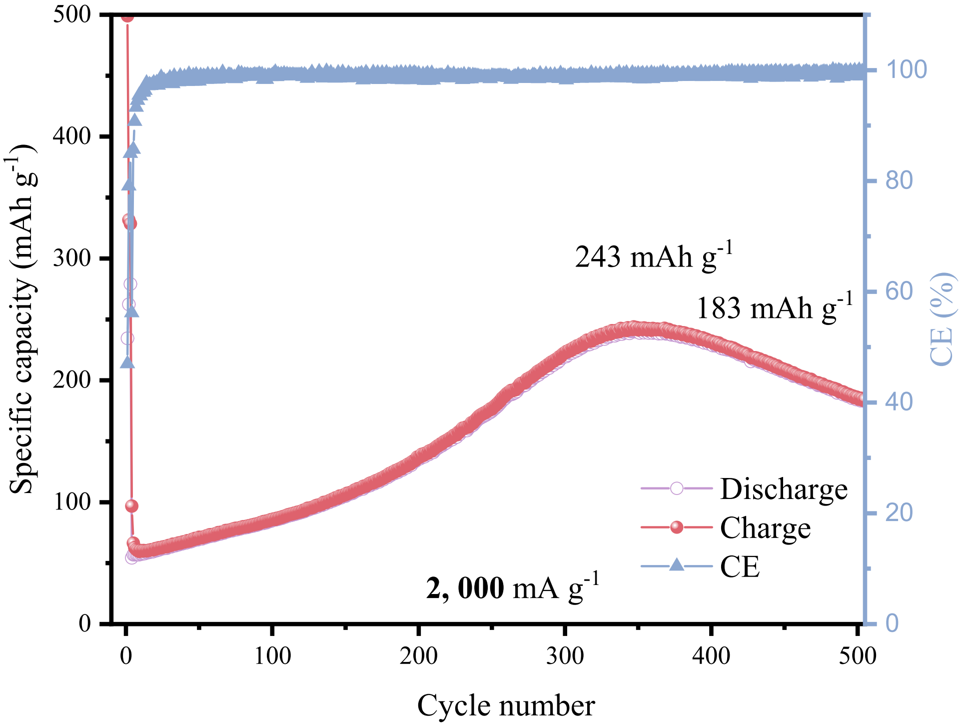

Fig. S27 Long-term cycle performances of the BIO anode at 2,000 mA g-1 after three-cycle activation.

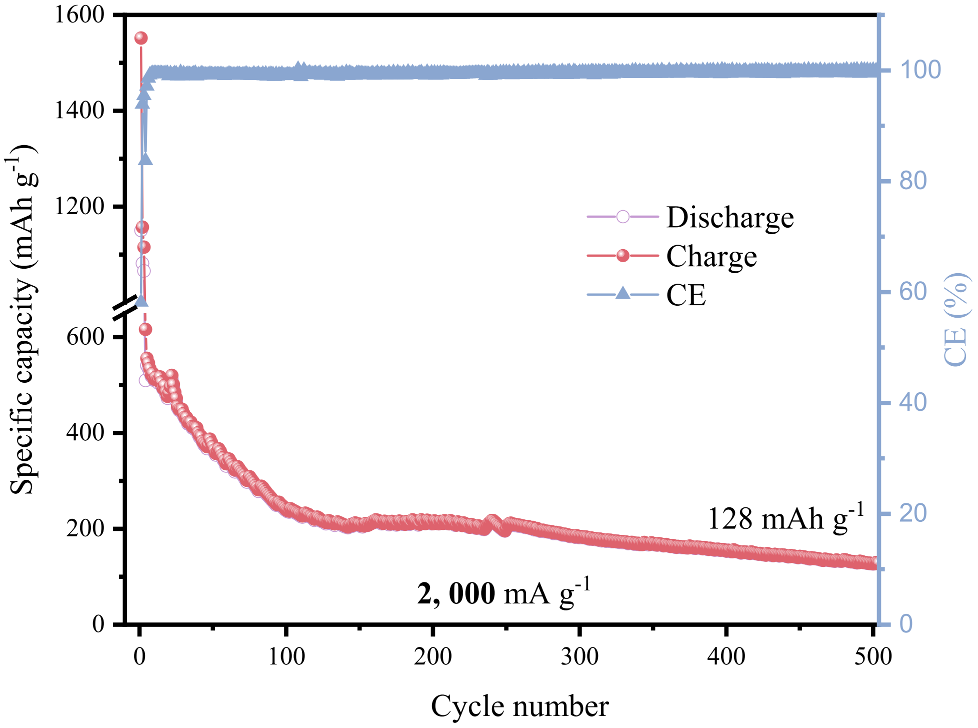

Fig. S28 Long-term cycle performances of the BIO/4C anode at 2,000 mA g-1 after three-cycle activation.

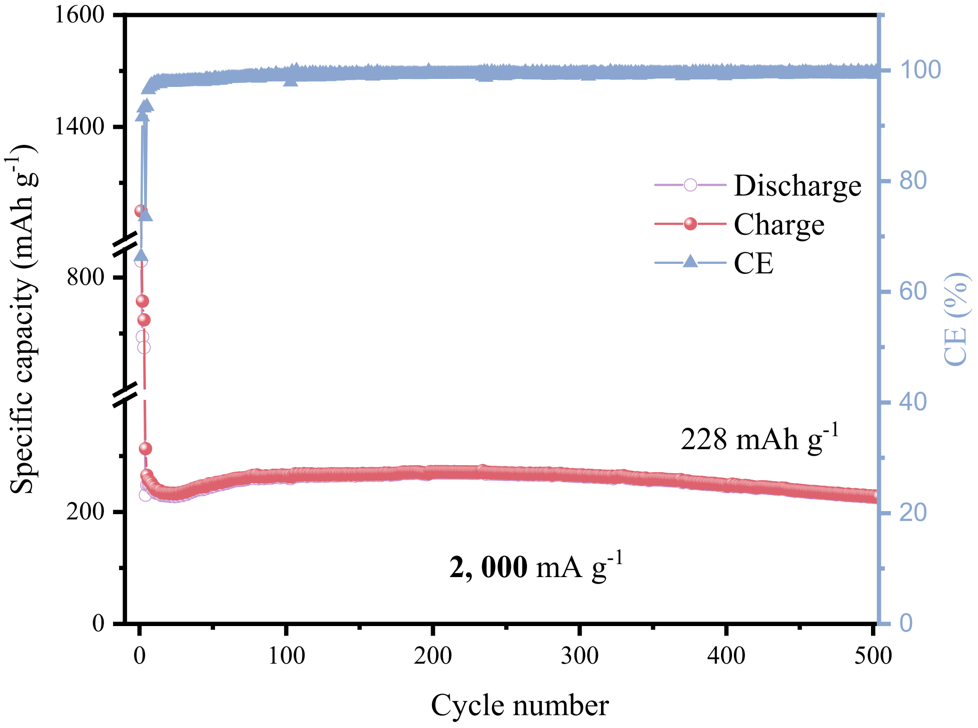

Fig. S29 Long-term cycle performances of the CNT anode at 2,000 mA g-1 after three-cycle activation.

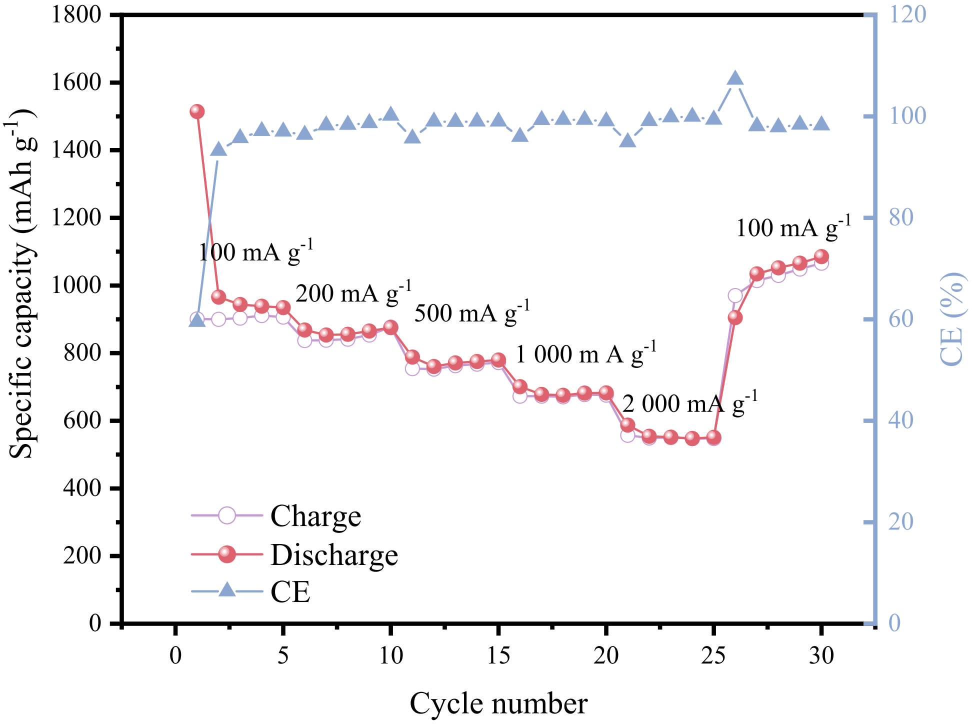

Fig. S30 The rate capability of the BIO-2C electrode at different current densities.

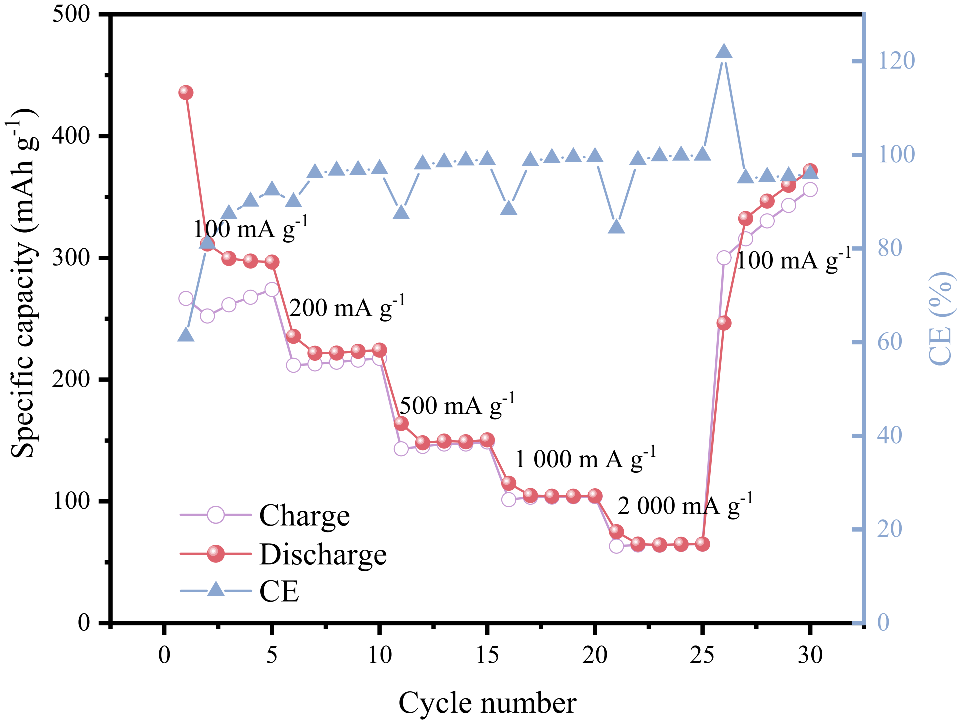

Fig. S31 The rate capability of the BIO electrode at different current densities.

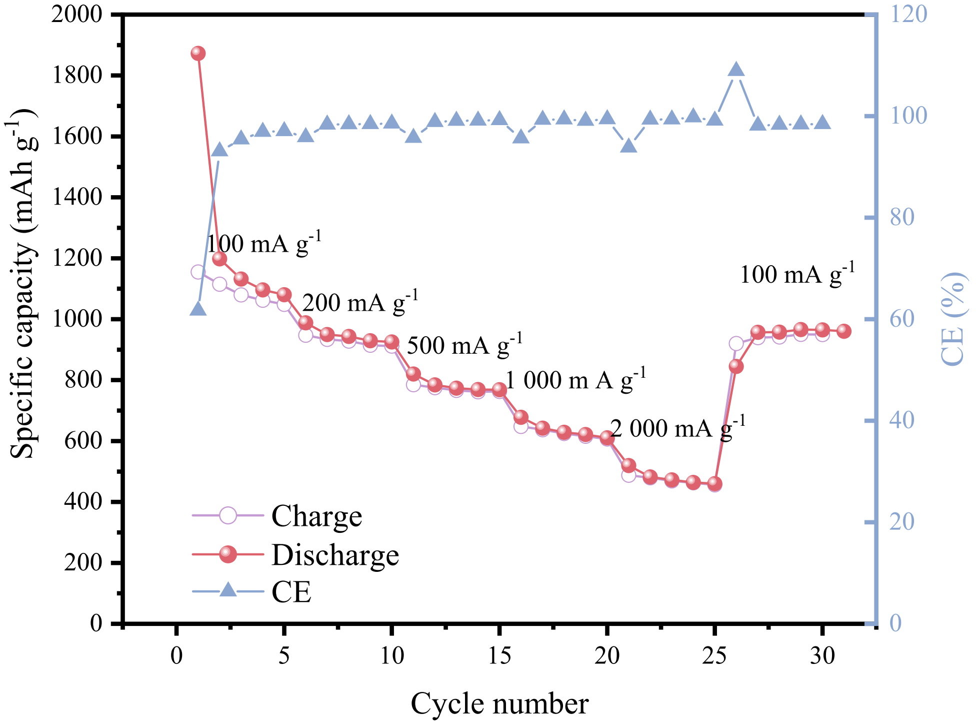

Fig. S32 The rate capability of the BIO/4C electrode at different current densities.

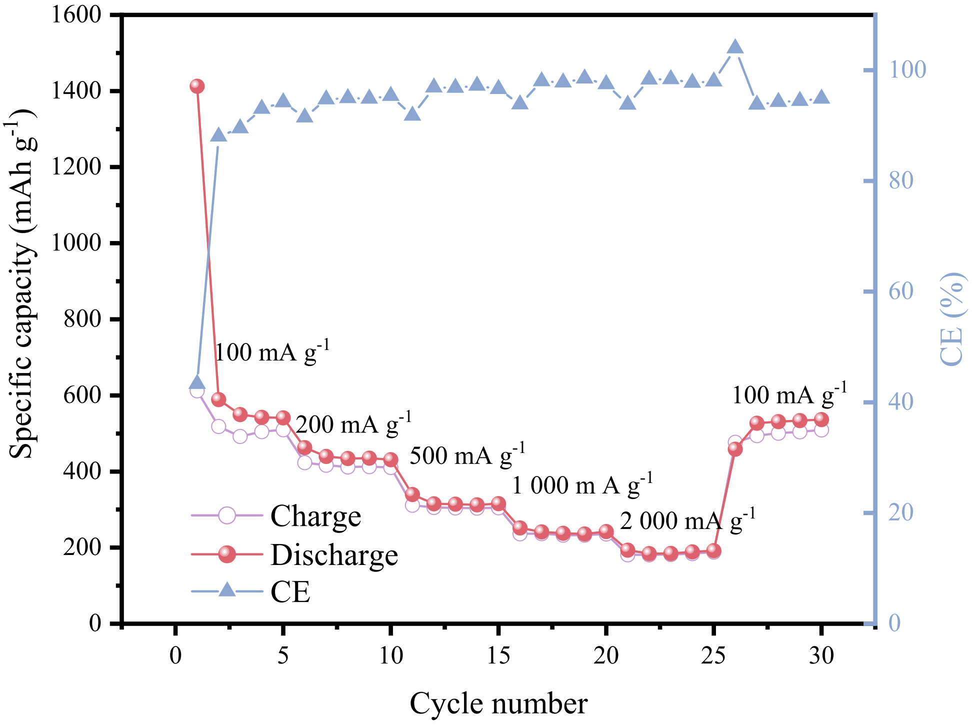

Fig. S33 The rate capability of the pure CNT electrode at different current densities.

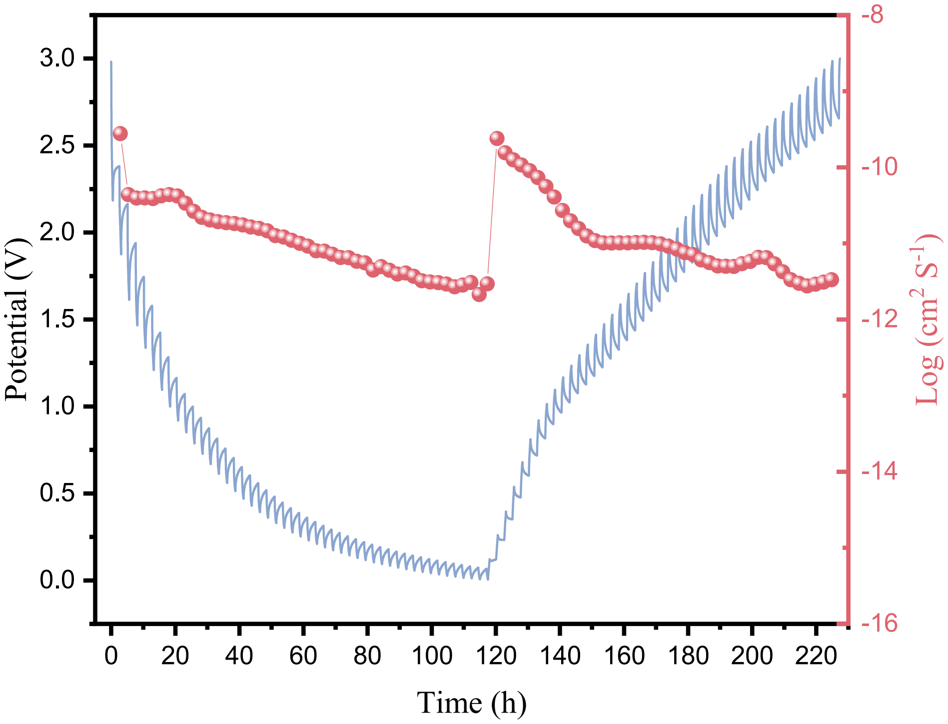

Fig. S34 GITT curve and diffusion coefficient of the BIO.

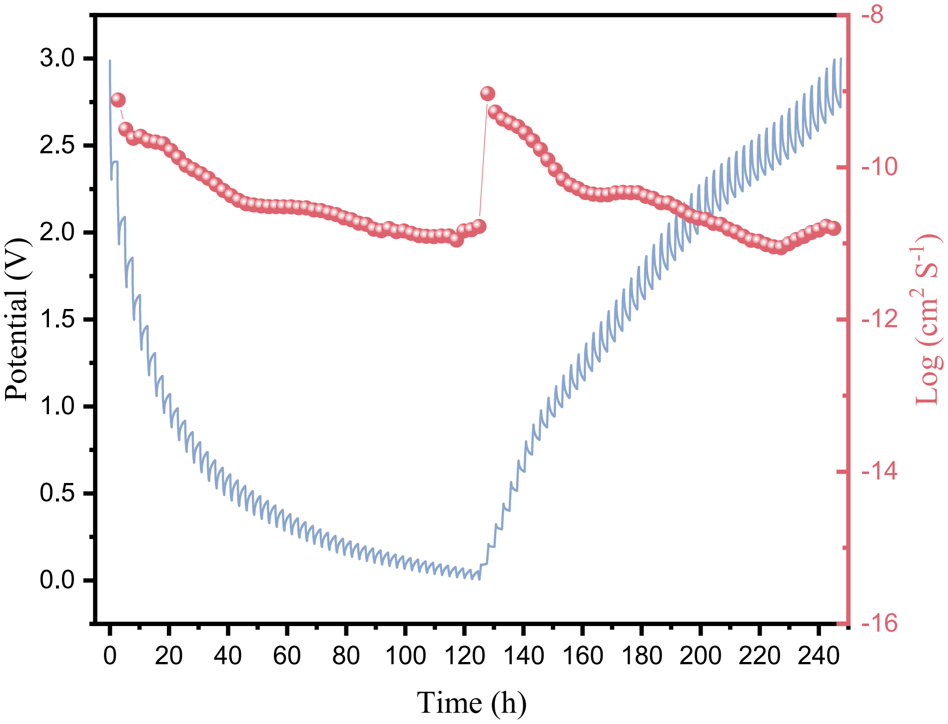

Fig. S35 GITT curve and diffusion coefficient of the BIO-2C.

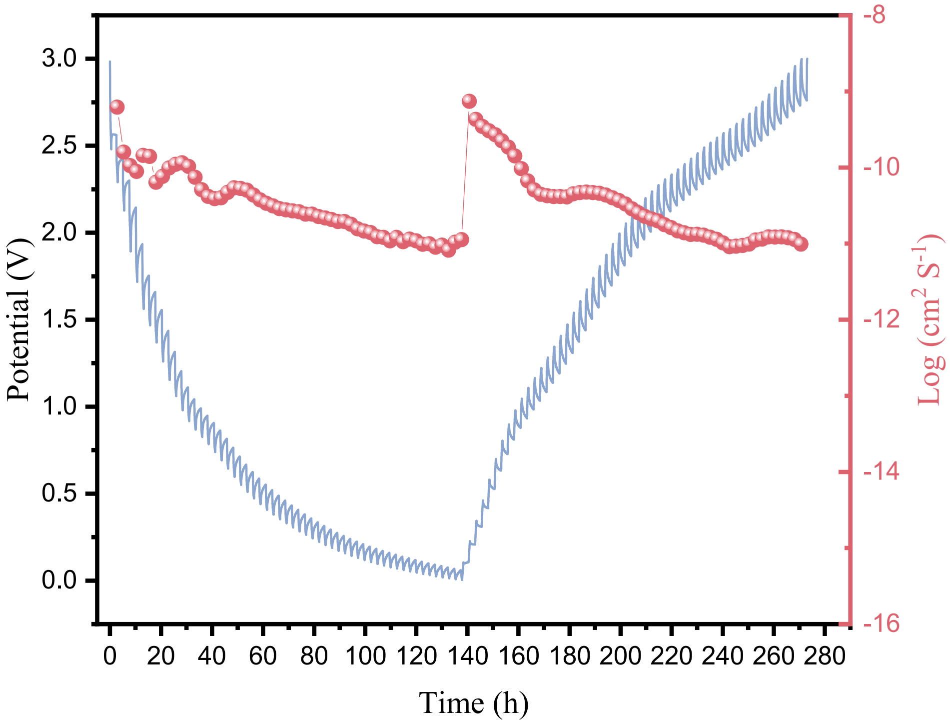

Fig. S36 GITT curve and diffusion coefficient of the BIO/4C.

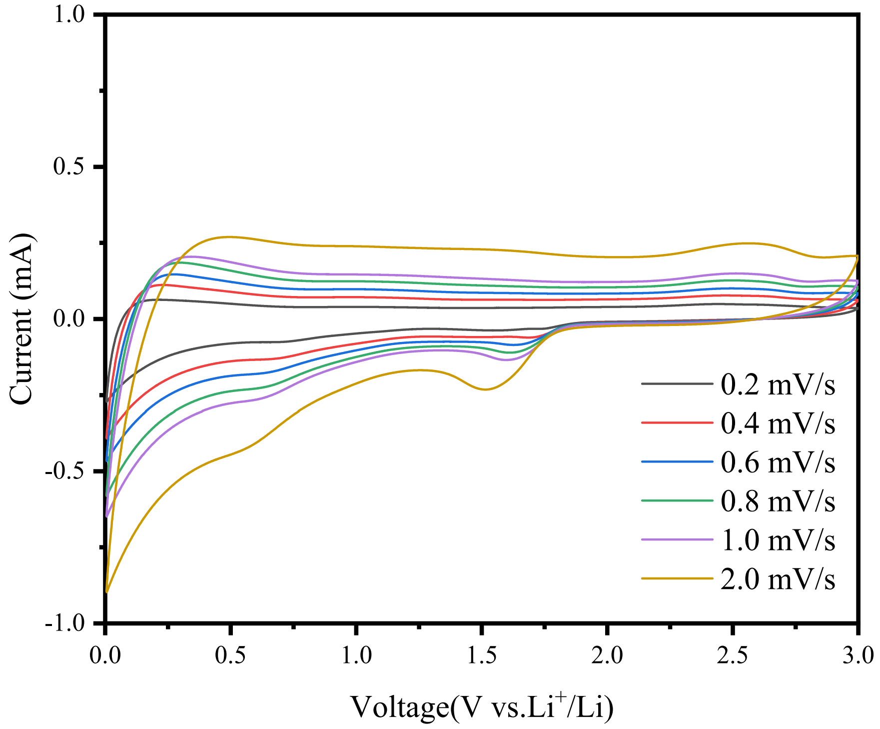

Fig. S37 CV curves of BIO anode at different scan rates (0.2, 0.4, 0.6, 0.8, 1.0, and 2.0 mV s^{-1}).

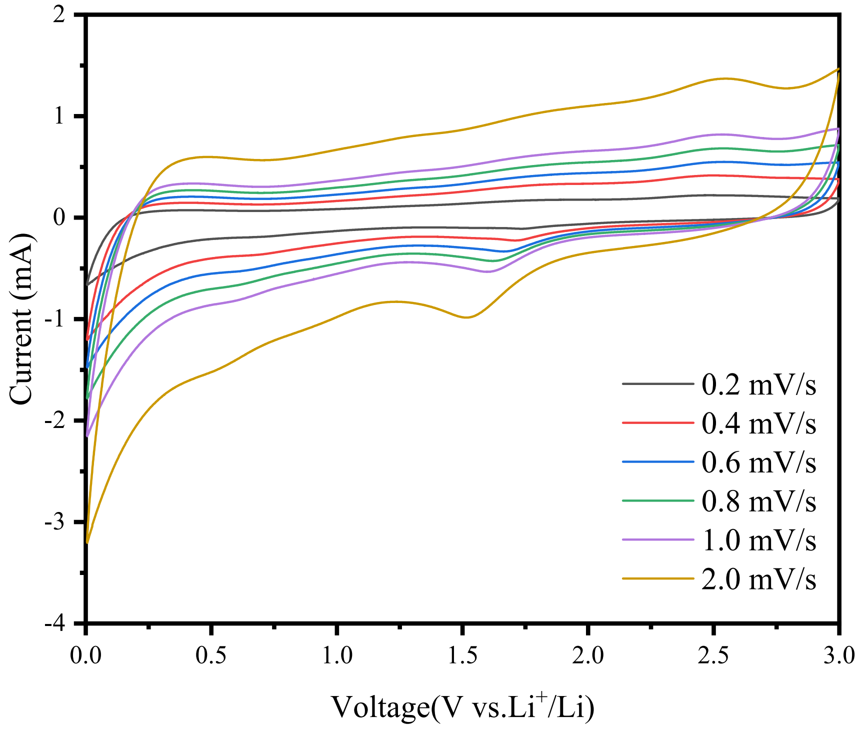

Fig. S38 CV curves of BIO-2C anode at different scan rates (0.2, 0.4, 0.6, 0.8, 1.0 and 2.0 mV s^{-1}).

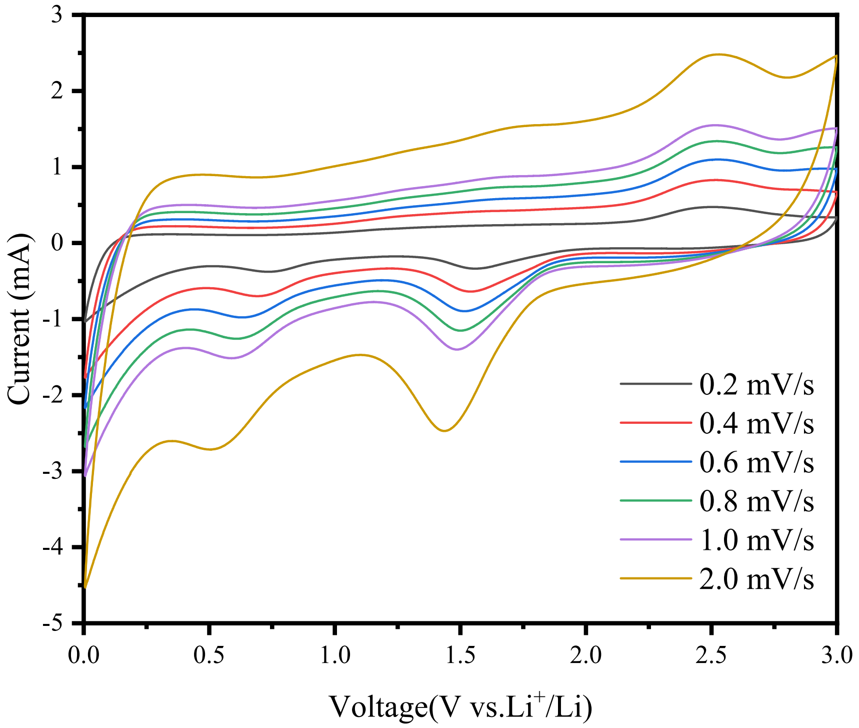

Fig. S39 CV curves of BIO-4C anode at different scan rates (0.2, 0.4, 0.6, 0.8, 1.0, and 2.0 mV s^{-1}).

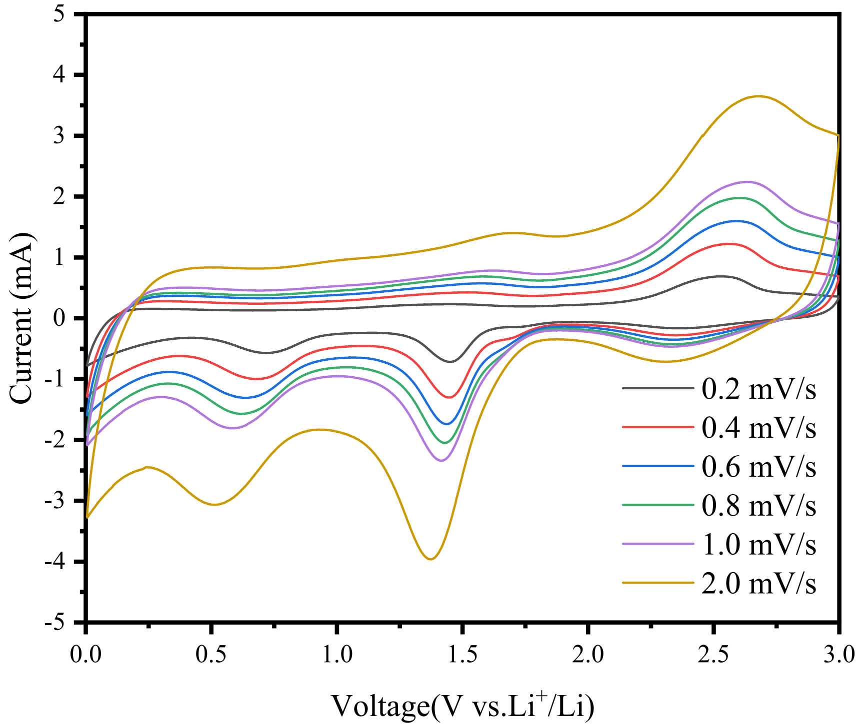

Fig. S40 CV curves of BIO/4C anode at different scan rates (0.2, 0.4, 0.6, 0.8, 1.0 and 2.0 mV s^{-1}).

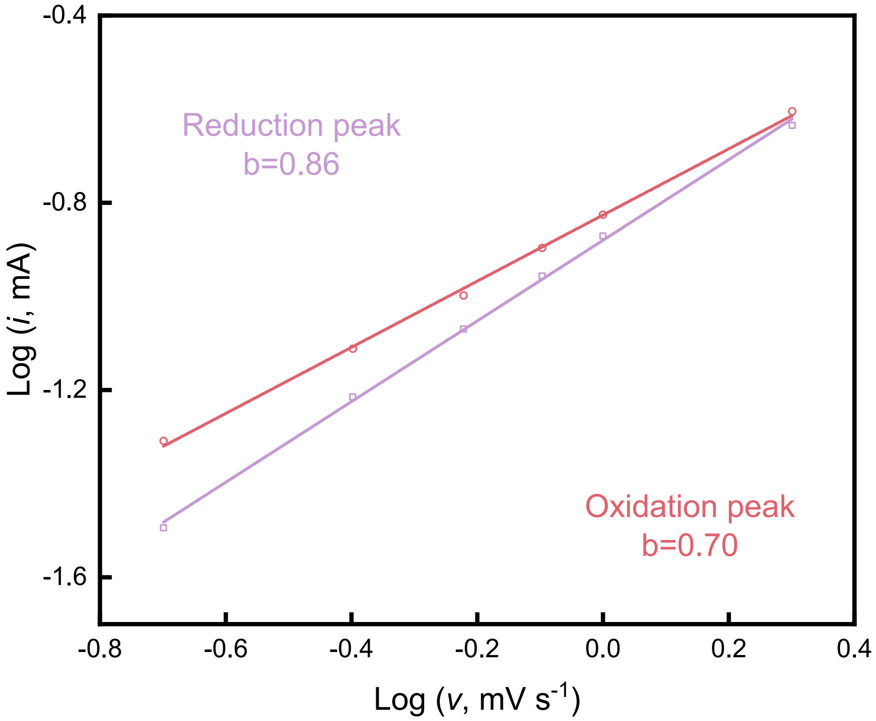

Fig. S41 The *b*-value of BIO representative reduction/oxidation peaks.

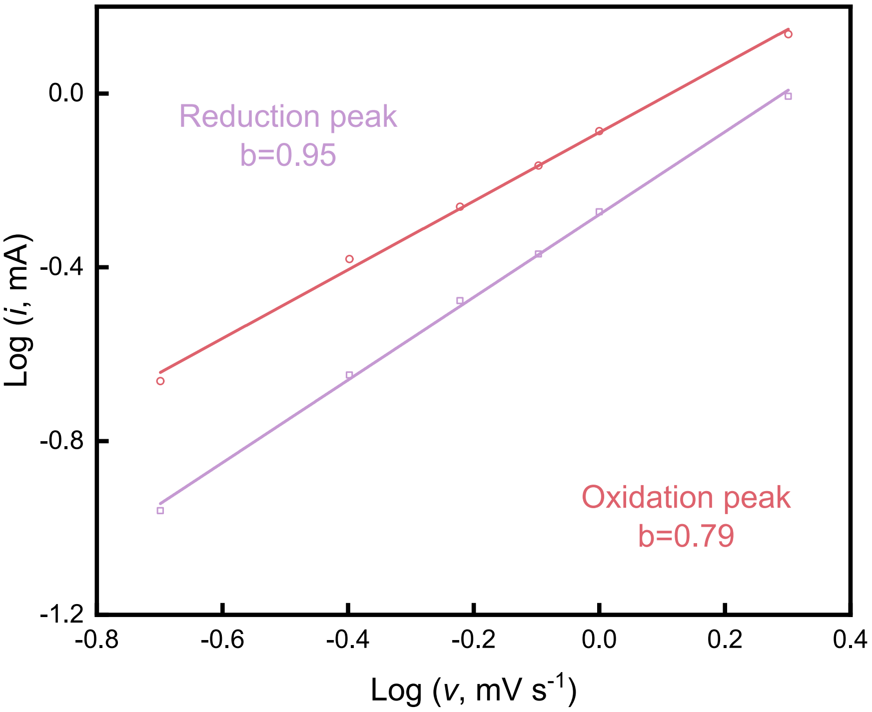

Fig. S42 The *b*-value of BIO-2C representative reduction/oxidation peaks.

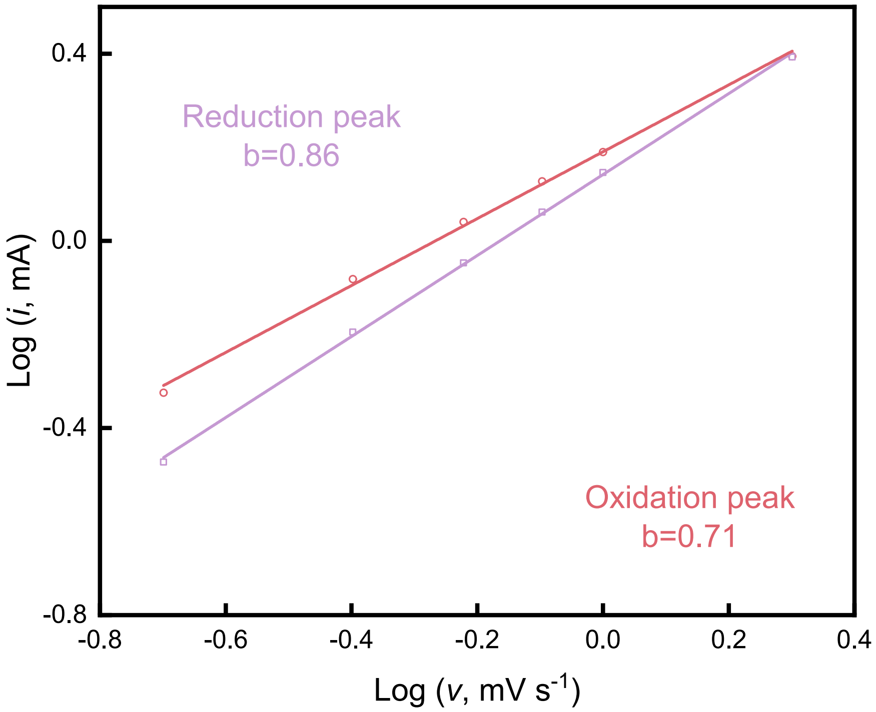

Fig. S43 The *b*-value of BIO-4C representative reduction/oxidation peaks.

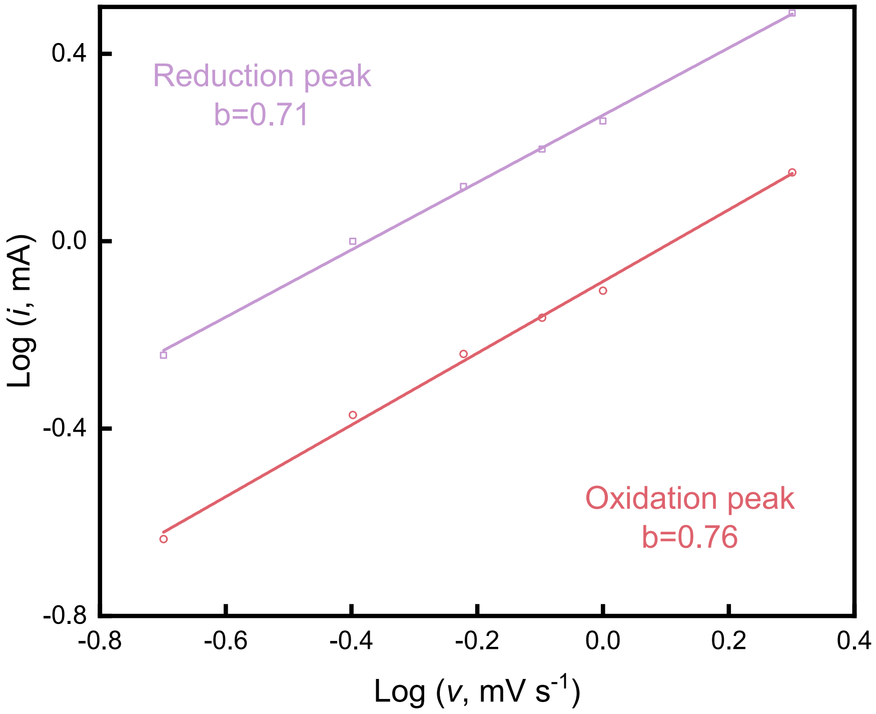

Fig. S44 The *b*-value of BIO/4C representative reduction/oxidation peaks.

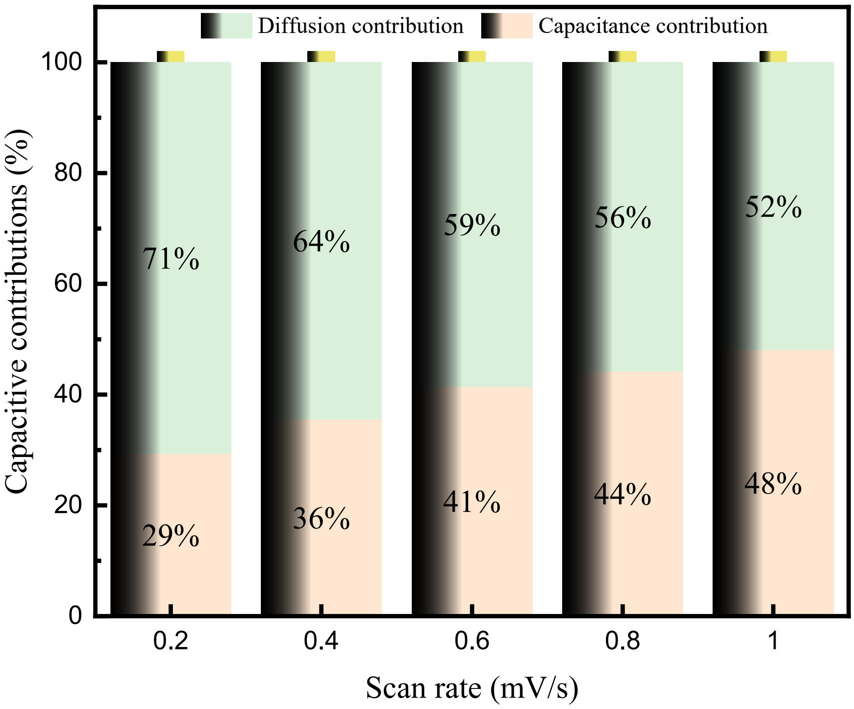

Fig. S45 Capacitive and diffusion contribution of BIO anode at multiple scan rates of 0.2-1.0 mV s^{-1}.

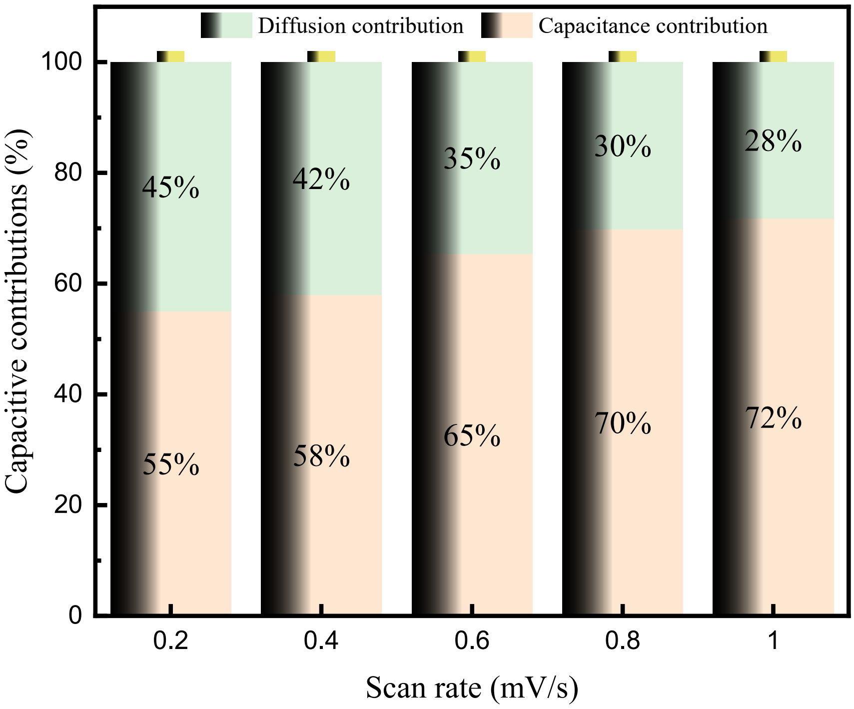

Fig. S46 Capacitive and diffusion contribution of BIO-2C anode at multiple scan rates of 0.2-1.0 mV s^{-1}.

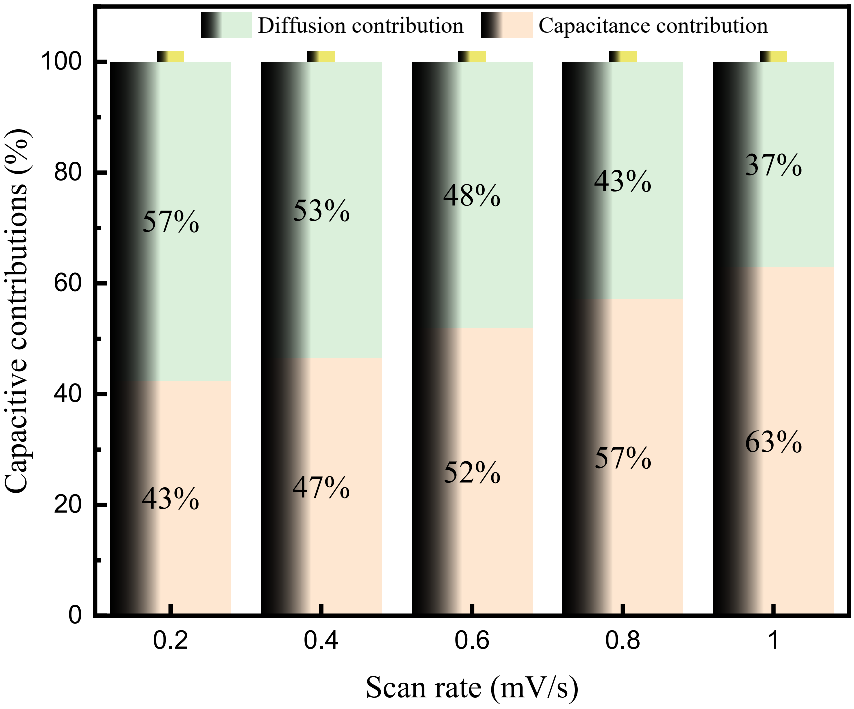

Fig. S47 Capacitive and diffusion contribution of BIO/4C anode at multiple scan rates of 0.2-1.0 mV s^{-1}.

10. X-ray Photoelectron Spectroscopy (XPS)

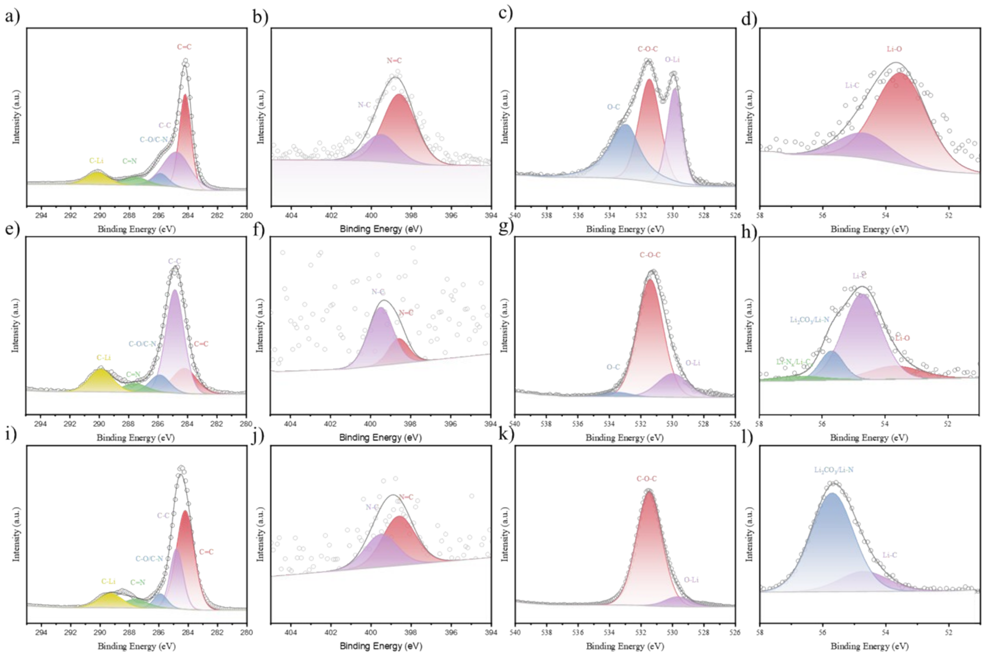

Fig. S48 XPS spectra of BIO-4C: (a-d) XPS spectra of the as-prepared the anode: (a) the C 1s scan; (b) the N 1s scan; (c) the O 1s scan; (d) the Li 1s scan; (e-h) XPS spectra of the lithiation of anode: (e) the C 1s scan; (f) the N 1s scan; (g) the O 1s scan; (h) the Li 1s scan; (i-l) XPS spectra of the delithiation of anode: (i) the C 1s scan; (j) the N 1s scan; (k) the O 1s scan; (l) the Li 1s scan.

11. Comparison of the Electrochemical Performances

Table S4 Comparison of the electrochemical performances of the CONs-based carbon materials for the anode of lithium-ion batteries in the literature.

Abbreviation for CONs-based anode	Capacity/Cycles (mA h g^{-1})	Current density (mA g^{-1})	Voltage range (V)	Ref.
BIO-4C	**364/504**	2 000	0.005-3.0	**This work**
BIO-2C	166/504	2 000	0.005-3.0	**This work**

BIO	183/504	2 000	0.005-3.0	**This work**
BIO/4C	128/504	2 000	0.005-3.0	**This work**
CTFs-1-400	740/1 000	1 000	0.005-3.0	1
CTFs-1-500	350/1 000	1 000	0.005-3.0	1
E-FCTF	581/1 000	2 000	0.005-3.0	2
PTZ-TFP-COF	391/2 000	1 000	0-3.0	3
Zn/Salen-PAF	218/2 000	5 000	0.01-3	4
TA-COF	227/2 000	5 000	0.01-3.0	5
Tf-TAPA	443/1 500	8 000	0.01-1.5	6
TFPPy-ICTO-COF	About 200/1 000	1 000	0.05-3	7
TpBpy	190/1 000	1 000	0.01-3	8
COF@CNT-2	373/2 000	1 000	0.01-3	9
CQN	451/1 000	1 000	0.01-3	10

Reference

1. F. Jiang, Y. Wang, T. Qiu, Y. Zhang, W. Zhu, C. Yang, J. Huang, Z. Fang and G. Dai, *ACS Appl. Mater. Interfaces*, 2021, **13**, 48818-48827.
2. H. Zhang, W. Sun, X. Chen and Y. Wang, *ACS Nano*, 2019, **13**, 14252-14261.
3. W. Li, W. Xie, F. Shao, J. Qian, S. Han, P. Wen, J. Lin, M. Chen and X. Lin, *Chem*, 2023, **9**, 117-129.
4. Q. Wang, Q. Chen, R. Zhao, H. Wang, W. Diao, F. Cui, S.-Y. Li, H. Wang and G. Zhu, *J. Colloid Interface Sci.*, 2023, **648**, 616-622.
5. Y. Tong, Z. Sun, J. Wang, W. Huang and Q. Zhang, *SmartMat*, 2022, **3**, 685-694.
6. Y. Zhang, Y. Wu, Y. An, C. Wei, L. Tan, B. Xi, S. Xiong and J. Feng, *Small Methods*, 2022, **6**, e2200306.
7. X. Xu, S. Zhang, K. Xu, H. Chen, X. Fan and N. Huang, *J. Am. Chem. Soc.*, 2023, **145**, 1022-1030.
8. S. Zhong, H. Zhao, Y. Ji, X. Li, T. Shu, Z. Cui and S. Liao, *J. Mater. Chem. A*, 2024, **12**, 11571-11579.
9. X. Yang, C. Lin, D. Han, G. Li, C. Huang, J. Liu, X. Wu, L. Zhai and L. Mi, *J. Mater. Chem. A*, 2022, **10**, 3989-3995.
10. F. Fang, Z.-T. Gong, L.-F. Yao, W. Pu, Y.-Q. Cai, Q.-L. Li, J.-J. Liu and S.-B. Xia, *J. Energy Storage*, 2023, **67**, 107521.